Hydrodynamics of Western Lake Erie During a Major Harmful Algal Bloom Event

by
Huayun Zhou

A thesis submitted
in partial fulfillment of the requirement
for the degree of
Master of Science of Conservation Ecology
(School for Environment and Sustainability)
in the University of Michigan
April 2019

Thesis Committee:

Dr. Dmitry Beletsky, chair
Prof. Bradley Cardinale
Dr. Thomas Johengen

Abstract

The breakout of a Harmful Algal Bloom (HAB) in Lake Erie in 2014 rendered Toledo without drinking water for three days. In 2015, Lake Erie subsequently experienced an even larger algal bloom. These societal and ecosystem impacts of HABs generated renewed urgency for HABs research to improve our understanding of the processes driving HAB development and our ability to better predict and manage them within the western basin of Lake Erie.

In this study, both observations and model simulations were used for analyzing circulation patterns responsible for promoting and transporting HABs within the western basin. Three surface drifters were released at the edge and inside the bloom in western basin Lake Erie in August 2015 that returned time and coordinates for data analysis. The observation data from surface drifters were used for validation of the hydrodynamic model Finite Volume Community Ocean Model (FVCOM) output. Next, wind and water levels were analyzed for the period of time when drifters were floating in the lake. To better understand the drifters' movements in the lake, a Lagrangian particle model, Process TRAJectory (PTRAJ), was forced by currents from FVCOM. The simulated virtual particle paths were then compared with the trajectories of the surface drifters. Different diffusivities were compared to assess the accuracy of the PTRAJ model. Finally, lake circulation and meteorological conditions were compared together for better understanding the physical processes that contribute to HABs development and transport. In particular, the wind has a significant impact on water transport from the nutrient-rich Maumee River estuary

towards the coastal regions that include the Toledo and Monroe water treatment plant intakes. Summer wind data for 2014, 2015, and 2016 were used to compare with western basin circulation. Sustained strong SE-S-SW winds and NE-N-NW-W winds were found most responsible for transporting water, as well as HABs, from Maumee Bay to Monroe and Toledo water intakes respectively.

Acknowledgment

I want to express sincere gratitude to my supervisor, Research Scientist Dima Beletsky, for his unwavering encouragement and hands-on guidance on hydrodynamic modeling. He is always patient in answering my questions and has motivated me tremendously for research and career planning as a scientist. I am immensely grateful for his help when I faced with difficulties in writing the thesis. I realized the area I need to improve for pursuing academic career path, and his wisdom in hydrodynamic modeling, as well as his attention to organization and details, will be a valuable treasure for me to continue my journey as a scientist.

At the same time, I wish to express my sincere thankfulness to my CIGLR colleagues, Eric Anderson, Mark Rowe, Thomas Johengen, Raisa Beletsky, and Bradley Cardinale, for their kind guidance and support on my research. I have leaned on their technical knowledge and expert insight on the Great Lakes

I am grateful to all GLERL and SEAS staffs for their support and help. Special thanks to Ms. Jennifer Taylor, Ms. Aubrey Lashaway, and Ms. Mary Ogdahl.

Finally, I am eternally indebted to my family and friends for their support and invaluable love. I want to add one more note for my violin, who always reminds me be brave and never give up.

Table of Contents

Nomenclature

BD	Bias deviation
DE	Distance Error
E	East
FVCOM	Finite Volume Community Ocean Model
GLERL	Great Lakes Environmental Research Laboratory
GLWQA	Great Lakes Water Quality Agreement
HABs	Harmful Algal Blooms
HRRR	High-Resolution Rapid Refresh
INTERP	Interpolated observations
N	North
NDBC	National Data Buoy Center
NE	Northeast
NOAA	National Oceanic and Atmospheric Administration
NW	Northwest
P/ TP	Phosphorous/ Total phosphorous
PTRAJ	Process TRAJectory
RMSE	Root Mean Square Error
S	South
SE	Southeast
SW	Southwest
W	West

List of Figures

List of Tables

Introduction

Harmful algal blooms (HABs), which are usually linked to anthropogenic eutrophication of waters, are of significant concern because of their adverse impacts to the water, lake ecosystem and society (Carrick, Moon, and Gaylord 2005; Hawley et al. 2006; Scavia et al. 2014; Rucinski et al. 2014; Rowe et al. 2016). Among the Laurentian Great Lakes, Lake Erie is susceptible to large blooms because of excessive anthropogenic nutrients, a warm temperature which is ideal for *Microcystis spp.* to grow because they have a higher temperature optimum (on the order of 25 ℃) than eukaryotic phytoplankton (Steffen et al. 2014), and lake circulation (Michalak et al. 2013; Beletsky, Hawley, and Rao 2013a). The reoccurring HABs in Lake Erie are generally observed from July to October and dominated by the species *Microcystis aeruginosa*. *Microcystis* produce microcystin, which belongs to a group of hepatotoxin compounds (Rowe et al. 2016). Besides toxins, the settling and remineralization of HABs may also contribute to hypoxia, a condition when the dissolved oxygen concentration is low, resulting in "dead zones" (Carrick, Moon, and Gaylord 2005; Hawley et al. 2006; Scavia et al. 2014; Rucinski et al. 2014).

Western basin of Lake Erie has severe HABs problems because it receives substantial nutrient load from its watershed, including two of its major tributaries: Detroit and Maumee Rivers (Figure 1). Maumee River is especially important source of nutrients because it drains a vast agricultural watershed and also urban centers in Ohio (Steffen et al. 2014). Bridgeman et al. (2011) showed that the Maumee River is not only an important phosphorous source but also a potential source of *Microcystis spp.* for the

lake. In contrast, although contributing a substantial portion of inflow into Lake Erie, the Detroit River has much lower nutrient concentrations (Bridgeman et al. 2012).

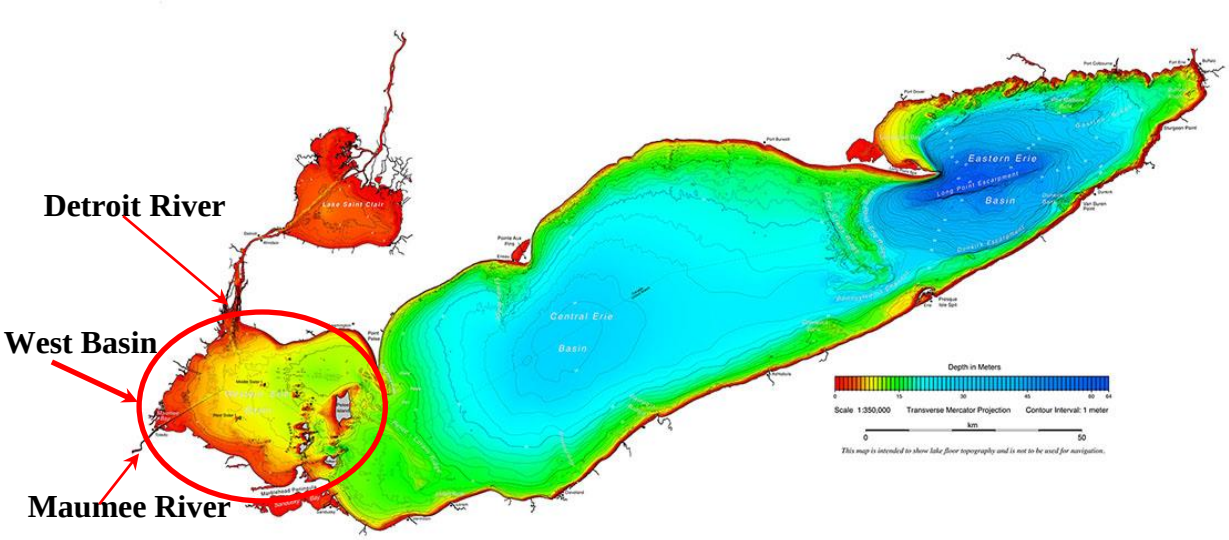

Figure 1. Lake Erie bathymetry.[1]

Frequent outbreaks of HABs in Lake Erie call for better management and prediction of HABs. Hydrodynamic modeling is an essential tool for HABs prediction because physical processes (e.g. advection by lake currents) have a significant impact on HABs development and spread in lakes. A previous study on summer circulation of Lake Erie had shown that circulation in the western basin, a basin mostly with no stratification, was driven by the Detroit River inflow and wind (Beletsky, Hawley, and Rao 2013b). Strong wind events significanty impact HAB's movement. Steffen et al. (2017) suggested that wind event moved the microcystin-rich water from Maumee Bay eastwards quickly reaching Toledo water intake.

[1] NOAA-GLERL Great Lakes bathymetry and shoreline data, see https://www.glerl.noaa.gov/data/bathy/bathy.html

Microcystin-rich water may adversely impact local water intakes causing significant issues with water supply. During the 2014 Toledo water crisis, the city was rendered without drinking water for more than two days (Henry 2014; Fitzsimmons 2014). Tens of thousands of people had to purchase bottled water because tap water was banned as a result of toxins harmful to human health found in the city water treatment plant. However, only three days before the tap water ban, there was no record of such toxin near the water intake at Toledo (See appendix A HAB Bulletin 2014) and that dramatic change stressed importance of accurate short-term HAB forecasting. Unlike seasonal HAB forecasts which rely primarily on nutrient loads, short-term forecasting relies more on physical transport than biological processes (Rowe et al. 2016). Early short-term forecasts used satellite imagery, meteorological forecast coupled with a hydrodynamic model and a Lagrangian particle tracking model for prediction of surface HABs advection (Wynne et al. 2011; Wynne et al. 2013). According to Wynne et al., the wind may have significant impact on vertical mixing, affecting the accuracy of model simulation. Rowe et al. (2016) improved a Lagrangian particle tracking model for the short-term forecast in Lake Erie by considering the vertical distribution of *Microcystis*. The model skill was influenced by several processes including advection, vertical mixing, and buoyancy, growth, and decay (Rowe et al. 2016). Short-term forecast of the Lake Erie HABs is available on the NOAA-GLERL website[2]. The Lake Erie HAB Tracker allows users to see when and where HABs are forming, providing useful guidance for HABs management.

[2] See: https://www.glerl.noaa.gov/res/HABs_and_Hypoxia/habTracker.html

While important for short-term HAB prediction, lake currents produced by circulation models were never directly tested with observations in western Lake Erie. Therefore, in 2015, three surface drifters that were taking records of time and location were released into the western basin of Lake Erie, providing observational data for validation of lake circulation produced by a hydrodynamic model FVCOM. FVCOM provides physical transport for the Lake Erie HAB Tracker and is also widely used in the Great Lakes modeling.

The goal of my M.S. thesis research was to gain insight into hydrodynamics of western Lake Erie during major HAB outbreak in 2015 using both observations and modeling, validate models with observations and also explore transport of water from Maumee Bay to water intakes of Toledo, OH and Monroe, MI. First, we analyzed drifter observations and used them in conjunction with water level data for the validation of a hydrodynamic model, FVCOM. Then we employed a Lagrangian particle model PTRAJ that uses FVCOM currents to simulate virtual particle movement, compare with drifter observations and test effects of horizontal diffusion on PTRAJ accuracy. Lastly, we explored wind conditions and resulting coastal circulation to learn which water intake would potentially be affected by HABs of Maumee Bay during sustained strong winds of particular direction.

Materials and Methods

1. Meteorological, Hydrodynamic and Satellite Observations

Surface Drifters

On August 19th, 2015, three surface drifters (Figure 2) were released in the Lake Erie western basin. Drifters were placed at the edge and inside of algal bloom. Each drifter had a GPS tracking device attached to the top, which reported locations to a satellite every hour. The data was tracked in near real-time and drifters were picked up when they hit the coastline.

Figure 2. Deploying drifters in Lake Erie Western Basin, August 2015: GLERL scientist E.J Anderson holds a drifter before it is released into the water.

Satellite imagery (cyanobacteria)

Chlorophyll-a, a pigment known to be related to the photochemical activity of photosynthesis (Strasserf, Srivastava, and Govindjee 1995), can be used as a proxy to evaluate the presence and the scale of the algal blooms in the lake basin. The presence of cyanobacteria and size of HABs in Lake Erie were analyzed using chlorophyll-a data obtained from satellite remote sensing imagery processed by NOAA GLERL.

Information on the chlorophyll-a was derived from NASA's MODIS-Terra data collected in summer 2015 during the period when the drifters were in the western Lake Erie. The process is based on an empirical relationship derived from *in situ* measurements of chlorophyll-a and blue to green band ratios of *in situ* remote sensing reflectances[3]. The colored pixels indicate the presence of cyanobacteria. Cooler colors such as blue or purple indicate low concentration and warm colors such as red, orange and yellow indicate high concentrations.

The images were obtained from the GLERL Harmful Algal Blooms in Lake Erie-Experimental and Operational HAB Bulletin Archive[4] (GLERL HABs bulletin) (See Appendix A HAB Bulletin 2015).

Water level and Wind

Lake Erie water level data were obtained from the NOAA Tides and Currents archive[5]. Hourly records from two gages were used for water level analysis, i.e., station 9063020 and 9063085 at Buffalo, NY, and Toledo, OH, respectively (Figure3).

---

[3] For more, see NASA MODIS: https://modis.gsfc.nasa.gov/data/dataprod/chlor_a.php

[4] See https://www.glerl.noaa.gov/res/HABs_and_Hypoxia/lakeErieHABArchive/

[5] See: https://tidesandcurrents.noaa.gov/

Hourly wind data were obtained from NOAA National Data Buoy Center (NDBC)[6] for buoy 45165 (Toledo water intake buoy at Oregon, OH), and buoy 45005, located just east of the western basin (Figure 3).

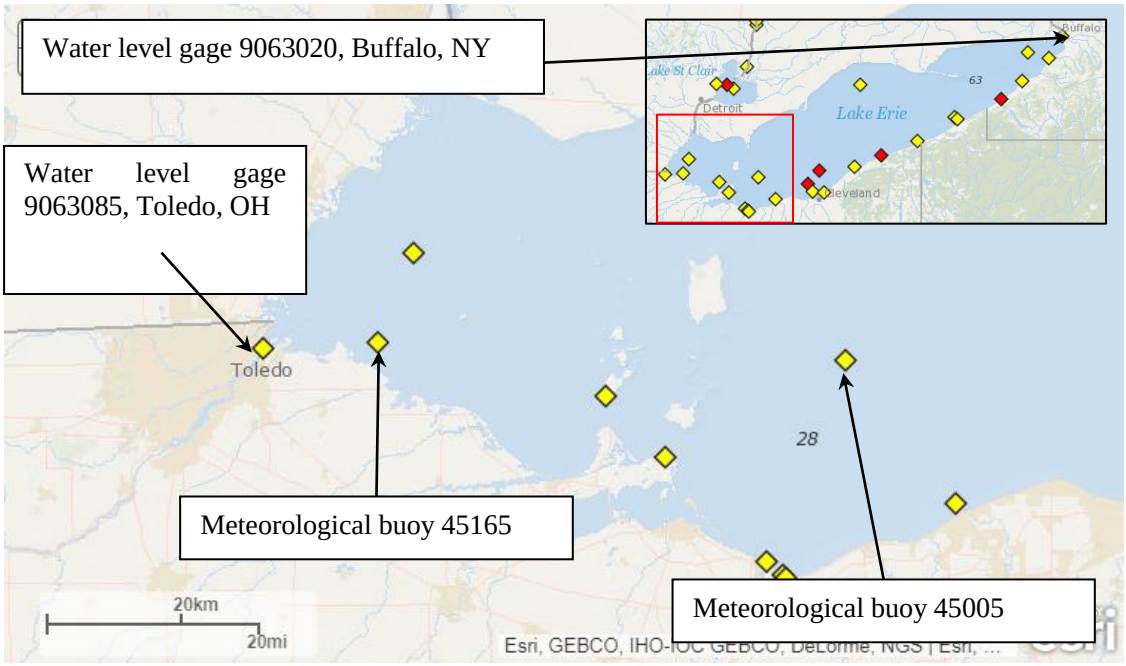

Figure 3. Lake Erie buoy and water level gage locations[7].

2. Drifter data processing

For velocity calculations, drifter coordinates were first converted from longitudinal and latitudinal values to Cartesian coordinates. Next, tracking time was converted from local time to UTC for future use in FVCOM validation (which output is UTC). Finally, drifter velocity components U and V, as well as speed, S, were calculated.

[6] See: http://www.ndbc.noaa.gov/

[7] NOAA-National Buoy Center, see https://www.ndbc.noaa.gov/

3. Hydrodynamic Model and skill assessment

3.1.Model Description

3.1.1. Hydrodynamic Model: FVCOM

Developed by Chen et al., FVCOM is a prognostic, unstructured-grid, finite-volume, free-surface, three-dimensional (3-D) model (Chen 2012). It solves the momentum, continuity, temperature, salinity, and density equations (Chen, Liu, and Beardsley 2003) and provides currents, turbulence, density and temperature as model output (Gilbert et al. 2010). FVCOM has an advantage for modeling domains with complex geometry and was quite successful in reproducing temperature and circulation in the Great Lakes (Anderson, Schwab, and Lang 2010).

The FVCOM output used in this analysis was obtained from two model runs using two alternative meteorological driving forces, i.e., INTERP and HRRR. INTERP is the observation based interpolated meteorological data and HRRR (High-resolution Rapid Refresh) model output is from NOAA real-time 3-km resolution, cloud-resolving, convection-allowing atmospheric model.

3.1.2. Lagrangian Particle Transport Model PTRAJ

The PTRAJ model is a 3D Lagrangian particle model developed to be used with FVCOM output by the UMASSD-WHOI. It is a part of FVCOM package and details can be found in Rowe et al., 2016, and at http://fvcom.smast.umassd.edu/. In this study we used PTRAJ in a 2D mode to simulate surface particles movements from 3 release points. The input files were hourly surface velocity components from FVCOM

run with HRRR forcing. The time step was 600s. The output time step was 1 hour. Horizontal diffusivity coefficients used: 0.0, 0.1, 0.5, 1.0, 2.0, 5.0, and 10.0 m^2/s.

3.2.Model skill assessment

The FVCOM model skill was assessed using bias deviation (BD), and root mean square error (RMSE) for scalar quantities.

$$\boldsymbol{BD} = \frac{\mathbf{1}}{\boldsymbol{n}}\sum_{\boldsymbol{i=1}}^{\boldsymbol{n}}(\boldsymbol{s_i} - \boldsymbol{o_i}) \quad \textbf{(1)}$$

$$\boldsymbol{RMSE} = \left[\frac{\mathbf{1}}{\boldsymbol{n}}\sum_{\boldsymbol{i=1}}^{\boldsymbol{n}}(\boldsymbol{s_i} - \boldsymbol{o_i})^{\mathbf{2}}\right]^{\mathbf{1/2}} \quad \textbf{(2)}$$

Vector quantities were assessed using the normalized Fourier norm (Fn) and the average angle difference $\langle\theta\rangle$ (Schwab 1983)

$$\boldsymbol{F_n} = \frac{\|\boldsymbol{v_o}, \boldsymbol{v_s}\|}{\|\boldsymbol{v_s}, \mathbf{0}\|} = \frac{(\frac{\mathbf{1}}{\boldsymbol{n}}\sum_{\boldsymbol{i=1}}^{\boldsymbol{n}}(|\boldsymbol{v_{oi}} - \boldsymbol{v_{si}}|)^{\mathbf{1/2}}}{(\frac{\mathbf{1}}{\boldsymbol{n}}\sum_{\boldsymbol{i=1}}^{\boldsymbol{n}}(|\boldsymbol{v_{oi}} - \mathbf{0}|)^{\mathbf{1/2}}} \quad \textbf{(3)}$$

$$\langle\boldsymbol{\theta}\rangle = \frac{\mathbf{1}}{\boldsymbol{\pi n}}\sum_{\boldsymbol{i=1}}^{\boldsymbol{n}}\boldsymbol{cos^{-1}}(\frac{\boldsymbol{v_{oi}}\cdot\boldsymbol{v_{si}}}{|\boldsymbol{v_{oi}}||\boldsymbol{v_{si}}|}) \quad \textbf{(4)}$$

where *s* and *o* represent simulated and observed values, respectively.

Fourier norm between 0 and 1 shows improvement of the model over no prediction, and the lower Fn, the better the model skill. Average angle difference with a value of zero shows perfect directional agreement.

Distance error (DE) metric was used to assess the PTRAJ model skill. It was calculated as a distance between observed and simulated drifter position at a particular moment in time.

$$\boldsymbol{DE} = \sqrt{(\boldsymbol{x_o} - \boldsymbol{x_m})^{\mathbf{2}} + (\boldsymbol{y_o} - \boldsymbol{y_m})^{\mathbf{2}}} \quad \textbf{(5)}$$

Results

1. Analysis of observations

1.1.Drifter and HABs Movement

Satellite imagery of chlorophyll-a in the surface water of western Lake Erie showed that the bloom started in mid-July and achieved maximum biomass in mid-August. At the time of drifter deployment (August 19, 105), the bloom was mainly observed along the southwest (SW) and northwest (NW) shore of western basin (Figure 4), with chlorophyll-a concentrations varying from 30 to 80 μg/L. Subsequently, the bloom expanded to the center of the Western basin and moved further eastwards. On Aug 22, the spatial extent of HABs increased, and the concentration of chlorophyll-a also increased: from 40 to 100 μg/L. On Aug 28, bloom along NW coast disappeared, but bloom moved to the central and east part of Western Basin and even expanded to Central Basin, with decreasing chlorophyll-a concentrations, around 20 to 80$-\mu$g/L. On August 31, the bloom stopped expanding to the east; however, algal concentration continued to increase with chlorophyll-a going varying between 40 and 400 μg/L. Notably, the bloom near South Bass Island started to clear after August 22 and disappeared by August 31.

Figure 4 showed drifter paths relative to the bloom and drifter location on days when satellite images were available during the 12 day period in August 2015. From August 19th to 31st, drifters moved eastwards and slightly to the north, while bloom movement was in the same direction. Initially, the drifters were released at the edge and inside the HABs, but when the drifters were collected, the drifters had moved out

of the HABs region, i.e., drifters moved faster than the bloom leading edge. Quite remarkably, while the drifters were released at different locations, they exhibited highly coherent movement moving in phase with a similar direction and speed (Figure 4).

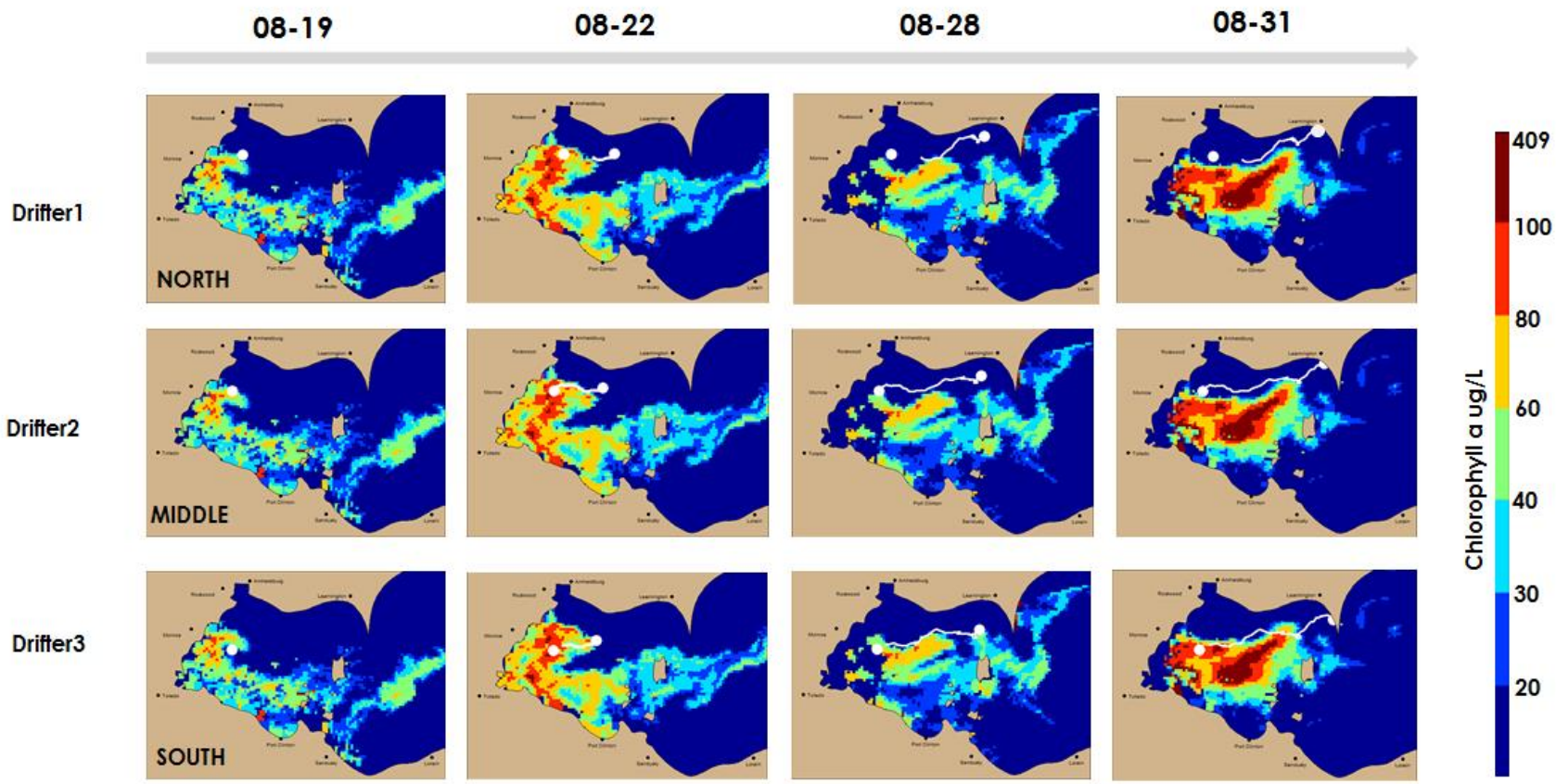

Figure 4. HABs and drifter movements in western Lake Erie 2015. The concentration of chlorophyll-a indicates the presence of algae in the water. Blue color indicates area with less chlorophyll-a, and red color indicates higher chlorophyll-a. The left white dot represents the initial release location of a drifter, and the right white dot represents the current location.

1.2. Surface currents derived from drifter data

Velocities derived from drifter positions exhibited periodic oscillations throughout the whole period of observations (Figure 5) with speeds up to 30 cm/s. East-west (U) component of velocity oscillations was substantially larger than north-south (V) component pointing out to a presence of longitudinal seiche. Previous research showed that a longitudinal seiche in Lake Erie is characterized by NE current followed by SW current, and so on. The slowest cycle, the first mode seiche has a period of about 14 h (Bolsenga and Herdendorf 1993). In our observations, we noted that currents spiked on day 236 (August 24) and resulting strong oscillations had a period of about 14 hours. We further explored the nature and specific characteristics of this energetic event in the next section.

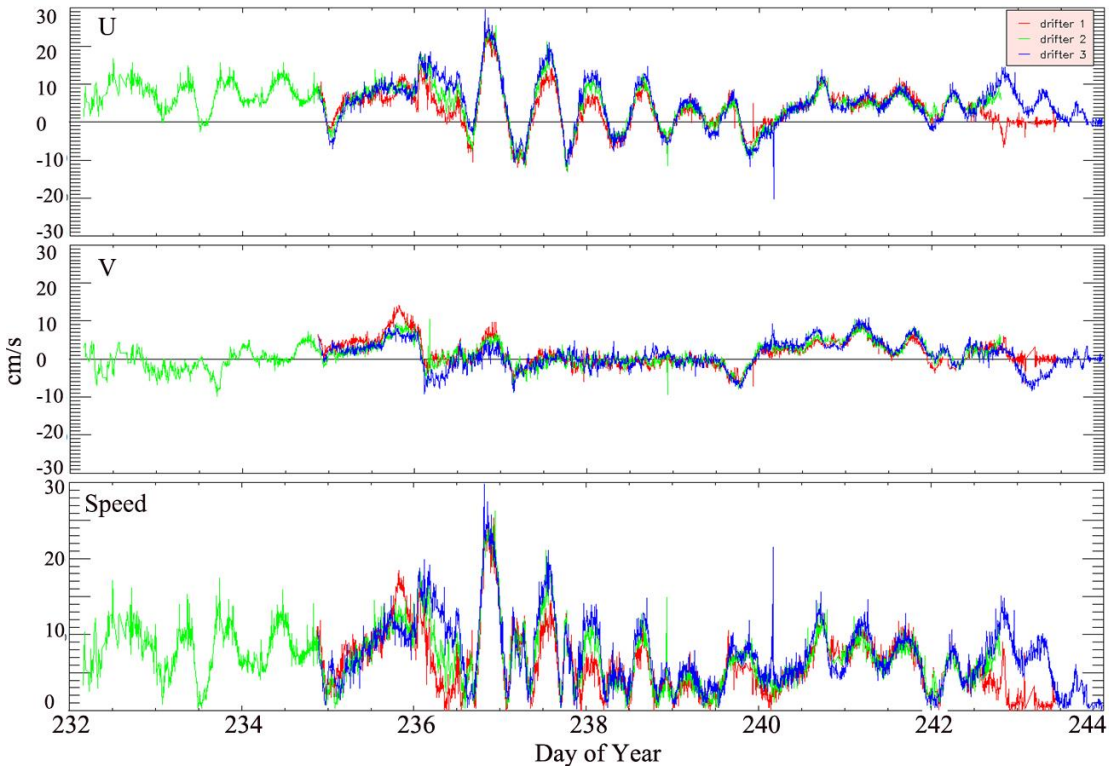

Figure 5. Velocity components and speed of drifters. Red, green and blue colors indicate Drifter 1, 2, 3, respectively[8].

[8] Three drifters were released on the same day, but for two of the drifters, we did not get much data for comparison on the first day.

1.3.Exploring a Wind Event

Observations of wind at the buoy near Toledo showed a strong wind event on day 236 (Figure 6). At the beginning of Day 236, there was a sudden change of wind from south-east to northwest, and then the wind direction gradually changed to the south-west. The wind speed increased from less than 5 m/s to around 7- 12 m/s.

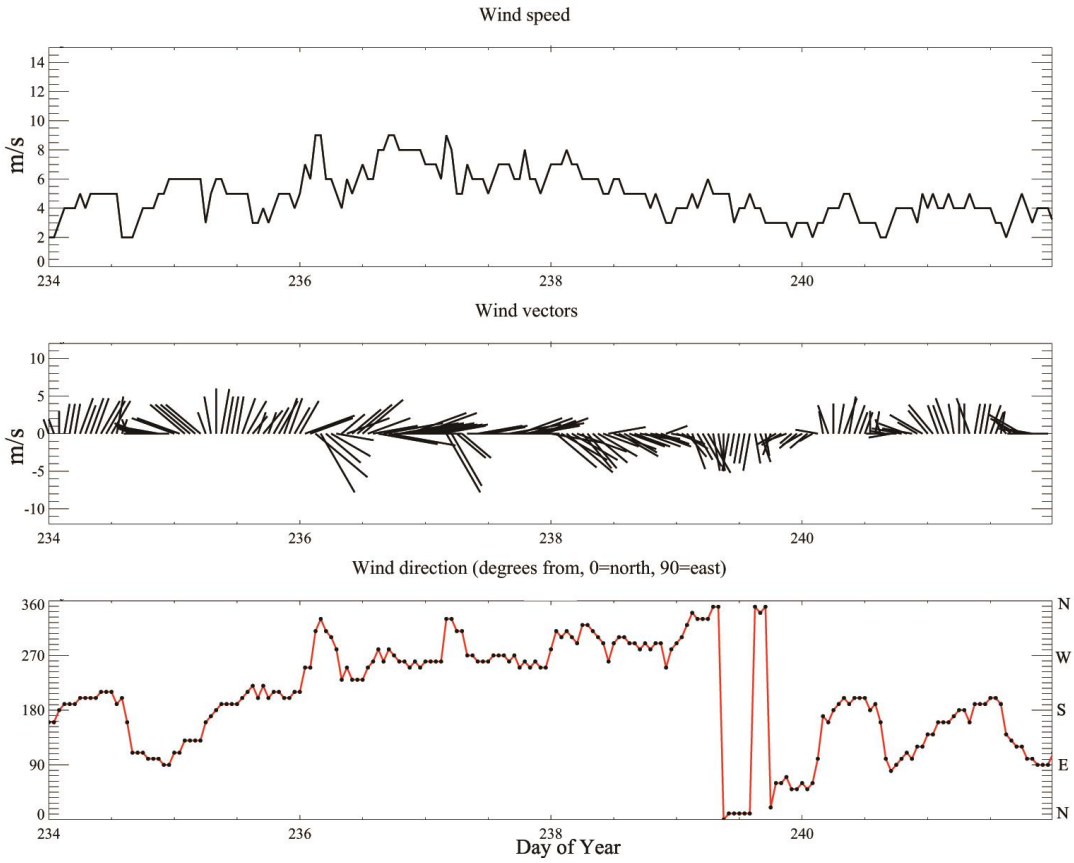

Figure 6. Observed hourly wind speed, bi-hourly wind vector and hourly wind direction during seiche event (buoy 45165 data).

For in-depth analysis of lake dynamics during the wind event we studied water levels observed at Buffalo and Toledo. Water levels at both stations had pronounced oscillations from day 236 to 240 (Figure 7). Notably, the oscillations of water level Toledo and Buffalo were in antiphase, with a period of ca. 14 hours, indicating a wind-induced seiche. After the first peak observed on day 236 the amplitude of oscillations gradually decayed.

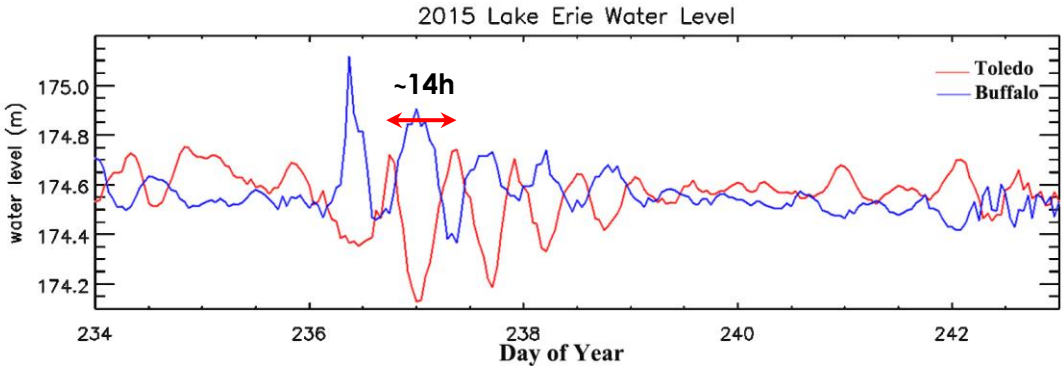

Figure 7. Observed Water Level at Toledo (red line) and Buffalo (blue line) during wind event in August 2015.

To explore the impact of velocity oscillations on drifter (and HAB) movements, the trajectories of three drifters were re-plotted focusing on the 4-day seiche episode (Figure 8). Trajectories showed back and forth east-west movements during days 237-240, consistent with the observations of water level and seiche characteristics while the net eastward movement was small. Circular drifter trajectories at the end of the episode suggested wind direction changes (indeed seen in Figure 6 around day 240).

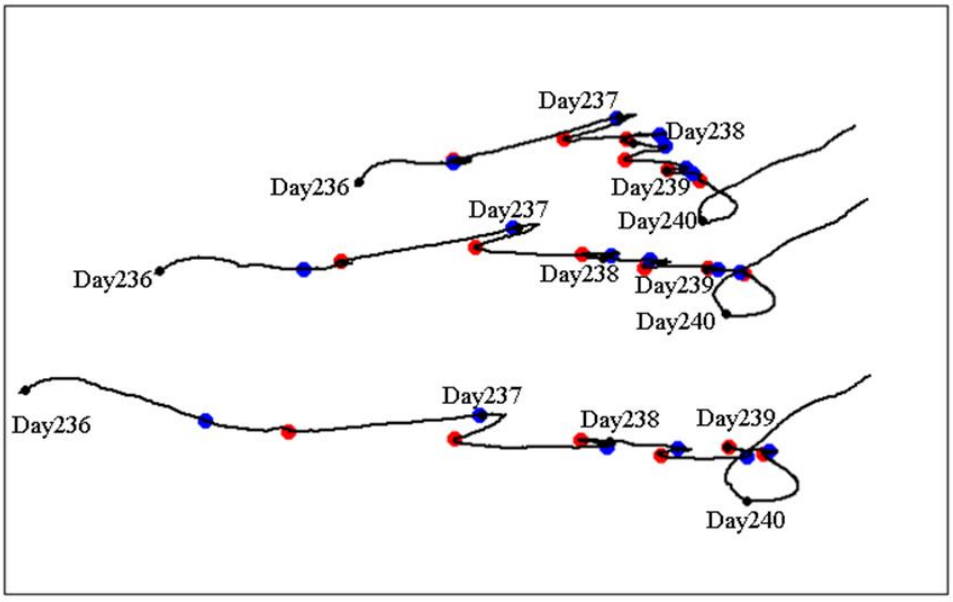

Figure 8. Drifter trajectories during seiche episode: days 236-240. Red and blue filled circles indicate Toledo water level peaks and troughs respectively, black filled circles mark days.

2. Hydrodynamic Modeling

2.1. FVCOM Results

Seiche-driven Circulation

To illustrate connection between circulation and water level dynamics during seiche event, modeled circulation was plotted along with the water level for a case of HRRR forcing. Surface circulation during opposite seiche phases is shown in top panels of Figure 9, while bottom panel of that figure showed the simulated water level. For example, when Toledo water level was rising, surface currents moved from Buffalo towards Toledo. In contrast, when Toledo water level was dropping, currents moved from Toledo towards Buffalo.

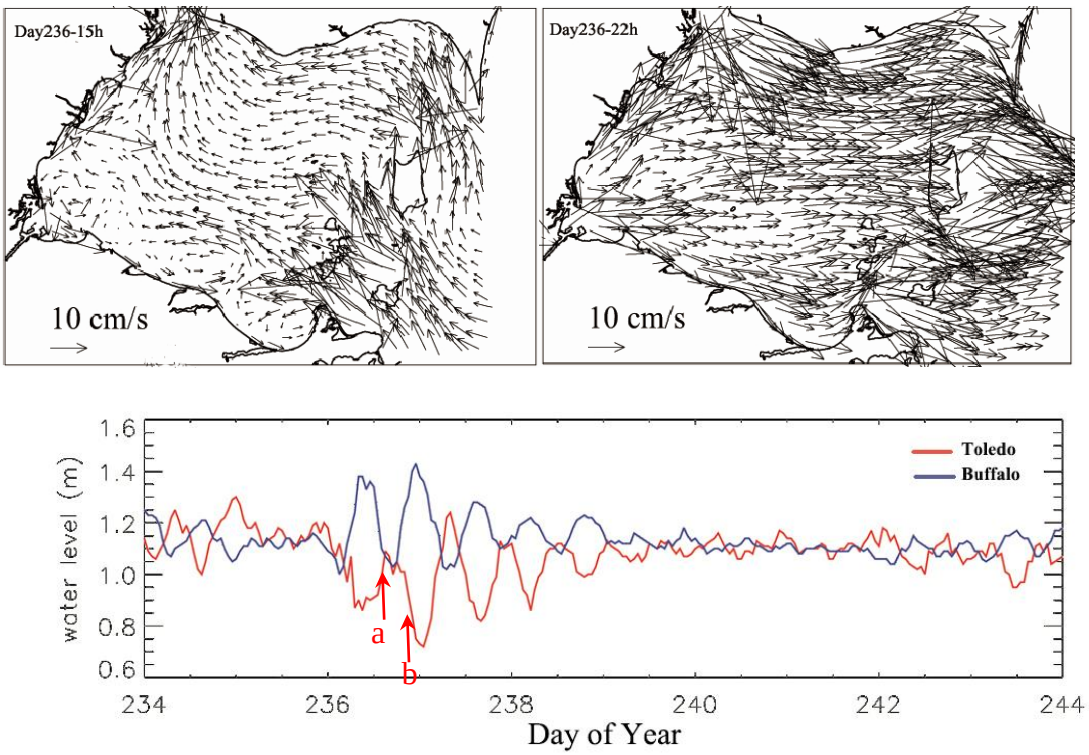

Figure 9. Simulated surface circulation (HRRR case) during different seiche phases (top two panels) and water level (relative to the mean lake level) at Buffalo (in blue) and Toledo (in red) (bottom panel) in August 2015. Arrows "a" and "b" in water level panel correspond to seiche phases shown in circulation panels.

Time-average circulation

Surface circulation was averaged over the 12-day period of drifter observations for both INTERP and HRRR model results (Figure 10). Both model runs predicted clockwise circulation in western basin. Currents flow eastward along southern shoreline, but there was also a small offshore anticlockwise gyre carrying currents westward to join the main clockwise circulation. The currents flowed eastward along the northern shoreline into the central basin. One significant difference between the two wind forcings is the direction of currents near the South Bass Island area. In the INTERP case, water flowed out of western basin into central basin. In contrast, water flowed from central basin into western basin in the HRRR case.

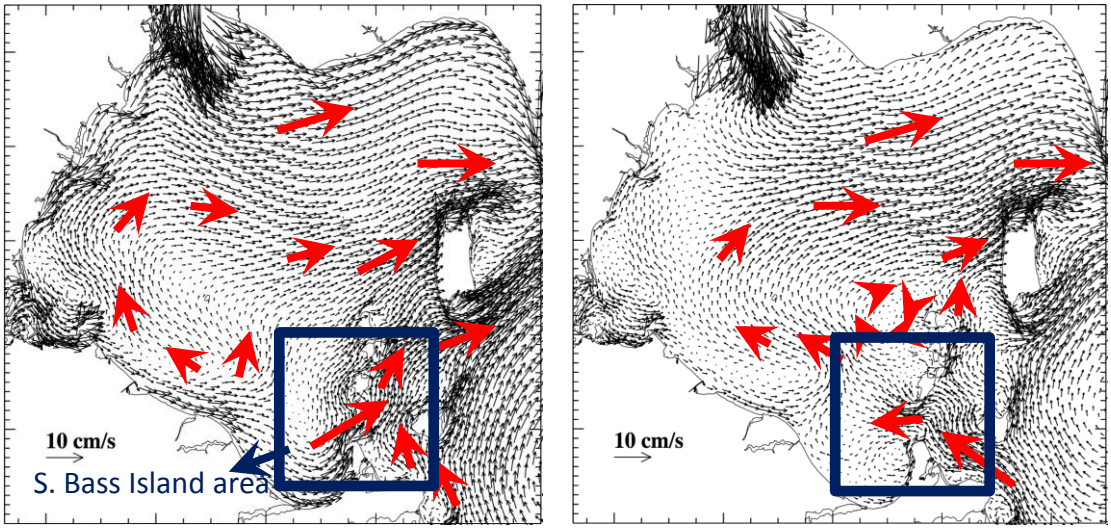

Figure 10. Modeled surface circulation (12-day average) when drifters were in the lake in August 2015, simulated by FVCOM with INTERP (left) and HRRR (right) forcing cases.

Model Validation

i. Validation of velocities and speed

Drifter 1 velocities and current speed based on observations and model simulations are shown in Figure 11 for both INTERP and HRRR cases. The model reproduced timing of oscillations well but underestimated its magnitude. Next, we calculated model skill statistics to compare the accuracy of INTERP and HRRR results quantitatively.

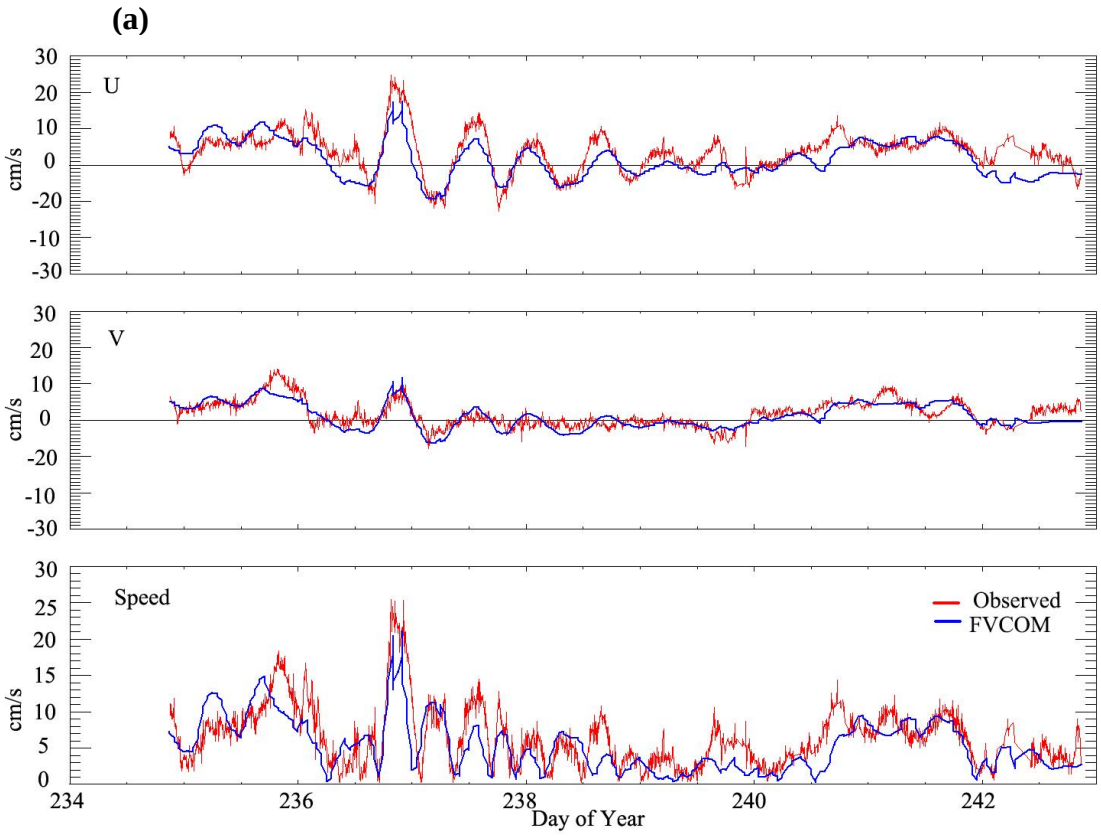

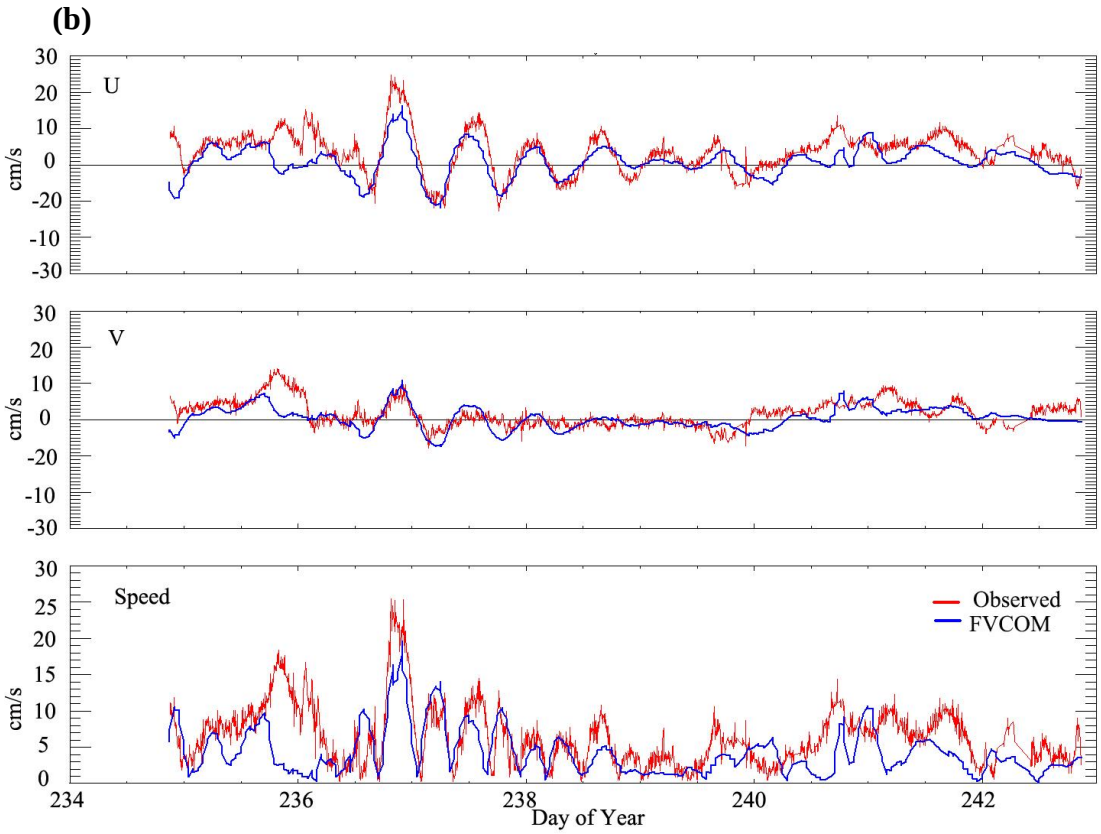

Figure 11. Modeled (blue) versus observed (red, derived from drifter 1 data) velocity components and speed. Subplot (a) shows results for INTERP case and (b) shows HRRR case (results for other drifters are in Appendix, Figure B.1).

First, linear regression was calculated using observed and modeled velocities and current speed (regression plots for both HRRR and INTERP cases are shown in Appendix, Figure B.2). For INTERP case, the R squares for U, V and S ranged across three drifters from 0.61 to 0.79, 0.47 to 0.79, and 0.23 to 0.73, respectively. For HRRR, the R squares for u, v and s ranged from 0.68 to 0.75, 0.34 to 0.57, and 0.50 to 0.63, respectively. No significant difference was found between INTERP and HRRR according to R square value according to simple regression model.

Results of statistical analysis for mean, BD, RMSE, Fn and average angle difference $\langle\theta\rangle$ are shown in Table 1. Results in bold indicate model runs with superior skill. INTERP showed a better result for both drifter 1 and drifter 2 with Fn of 0.60 and

0.69, and $\langle\theta\rangle$ of 45 ° and 41 °, respectively. HRRR showed a better result for drifter 3, with an Fn of 0.7 and $\langle\theta\rangle$ of 44 °. As for BD, INTERP showed better results for drifter1 and drifter 2, and HRRR shows better results for the drifter 3. Overall, the BD, RMSE, and Fn between two model cases are comparable with no clear advantage of particular forcing for current predictions in the northern part of western basin where observations were made.

Table 1 Model-data comparison of the velocity (U, V) and current speed (S) in Lake Erie Western Basin for drifters D1, D2, and D3.

		Observations	**INTERP**					**HRRR**				
		Mean cm/s	mean cm/s	BD cm/s	RMSE cm/s	Fn	$\langle\theta\rangle$	mean cm/s	BD cm/s	RMSE cm/s	Fn	$\langle\theta\rangle$
D1	U	3.5	1.7	**-1.9**	**4.0**	**0.60**	**45 °**	0.7	-2.8	4.8	0.76	48 °
	V	1.8	1.2	**-0.6**	**2.4**			0.4	-1.4	3.4		
	S	6.5	5.4	**-1.1**	**3.1**			4.4	-2.1	4.4		
D2	U	5.1	2.4	-2.7	5.0	**0.69**	**41 °**	2.4	-2.7	5.0	0.73	44 °
	V	1.0	1.0	**0.0**	**2.9**			1.1	0.1	3.4		
	S	7.3	5.8	**-1.4**	**4.3**			4.9	-2.3	4.4		
D3	U	4.9	1.8	-3.2	6.2	0.81	48 °	2.4	**-2.6**	**4.8**	**0.70**	**44 °**
	V	1.1	0.6	-0.5	3.7			1.4	**0.3**	3.7		
	S	7.7	5.8	**-1.8**	5.3			5.0	-2.7	**4.4**		

Note: Fn-Fourier Norm, Fn = 0, perfect agreement between simulated and observed currents, values between 0, 1 indicate improvement over no prediction.
Angle error $<\theta>$, average difference, a value of 0 implies perfect directional agreement (Schwab 1983).
D1, D2, and D3 represent drifter 1, 2, and 3.

ii. Validation of water level

Observed water level at Toledo and Buffalo was plotted against INTERP and HRRR model results (Figure 12). Similar to velocity, the model reproduced timing of events well but underestimated magnitude. Simple regression analysis was conducted for both INTERP and HRRR cases (see Appendix B.3).

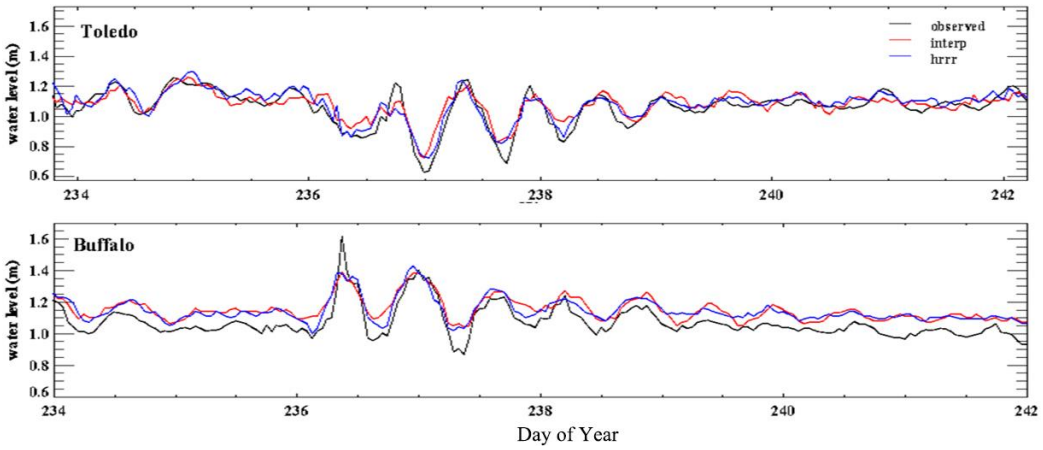

Figure 12. Observed (black) versus modeled (red – INTERP, blue-HRRR) water level at Toledo (top panel) and Buffalo (bottom panel) in August 2015.

According to statistical analysis (Table 2), R squares in INTERP case were 0.75 and 0.91 at Buffalo and Toledo respectively and 0.75 and 0.94 in HRRR case. The p-values for both models were less than 2.2e-16. Higher R square indicated that the HRRR model performed slightly better than the INTERP model in water level simulations.

Table 2 Statistics of water level between observation and model results

	INTERP		**HRRR**	
	R square	P value	R square	P value
Buffalo	0.75	<2.2e-16	0.75	< 2.2e-16
Toledo	0.91	<2.2e-16	0.94	<2.2e-16

Overall, INTERP and HRRR did not show a big difference in the accuracy of velocity and speed predictions. However, HRRR does better than INTERP in water level simulation.

2.2.PTRAJ Results

In the previous section, FVCOM surface current errors were estimated using drifter observations. In this section, we want to address a related question: what spatial errors occur when FVCOM output is used to predict the movement of drifters in Lake Erie using particle-based models (Lagrangian models). This is particular important for HAB forecasting. To address this question virtual particle trajectories were simulated with PTRAJ using results from FVCOM simulation (HRRR case). To find the optimal diffusion coefficient to match observations (i.e. drifter path) better, the PTRAJ model was run multiple times with different horizontal diffusivities, i.e. 0, 0.1, 0.5, 1.0, 2.0, 5.0 and 10.0 m^2/s.

Figure 13 shows observed drifter 1 trajectories together with the modeled drifter trajectories simulated with horizontal diffusivities of 0, 0.5, 1 and $10m^2/s$. According to PTRAJ results, the virtual particles moved in the same direction as compared with the real drifter trajectories. However, regardless of diffusivity choice, the model underestimated the distance traveled by the drifters (in line with previously reported slower modeled currents), and all virtual drifters reached the shore about a week later than the drifters deployed in the lake.

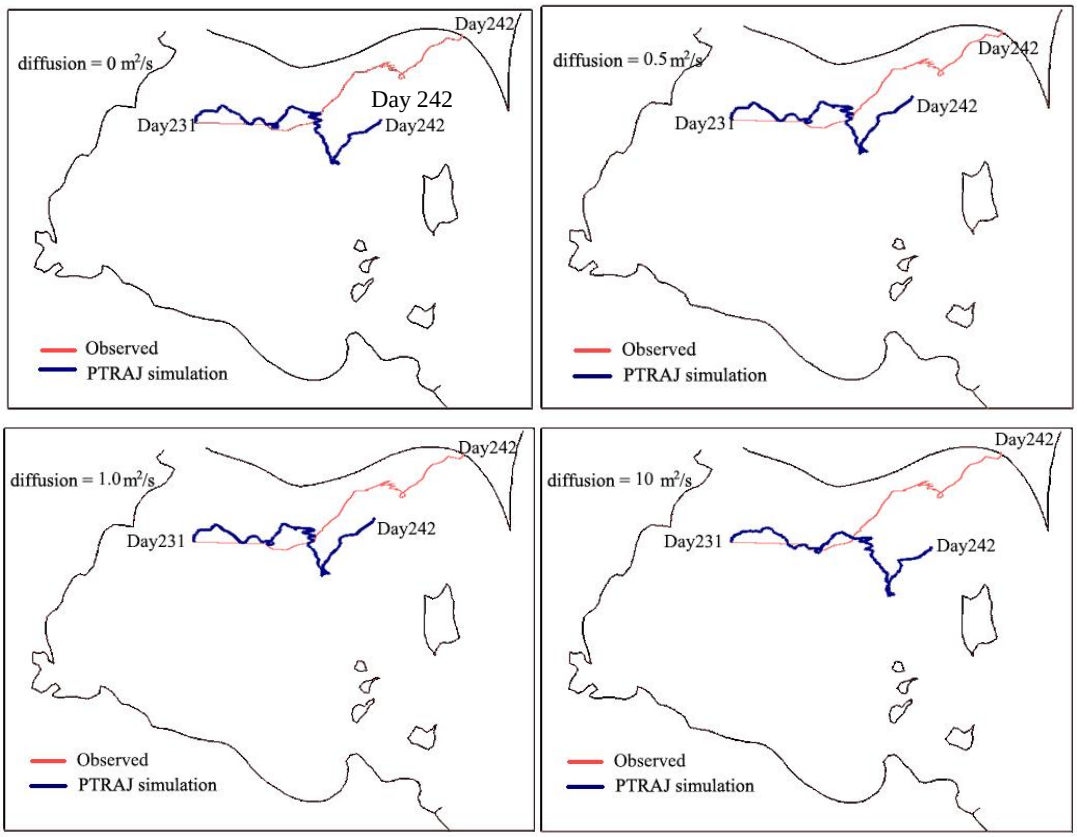

Figure 13. Observed (red) versus PTRAJ simulated (blue) drifter 1 trajectories (diffusivity = 0, 0.5, 1, and 10 m2/s) in August 2015.

To quantify spatial model error, the separation distance error was calculated using simulated (hourly) drifter positions and the observed drifter positions. The results for drifter 1 were shown in Figure 14 for different horizontal diffusion values. The black line showed zero diffusion case; red, orange, green, dark blue, purple and light blue shows simulation with diffusion 0.1, 0.5, 1.0, 2.0, 5.0 and 10.0 m^2/s, respectively.

The results showed that the distance errors had some variability depending on diffusion coefficient but grew in time in all cases during the 12 day simulation period. The increase was not always steady though. Distance error increased linearly for the first two days of simulation but then did not change much for the following two days. There was a steep increase in error on day 236 coinciding with strong wind event

discussed earlier and another steep increase on day 240 when wind speed and direction changed drastically again. Distance error started to decrease at the end of the simulation (as drifter was approaching the shore where it beached) after reaching its maximum on day 242.

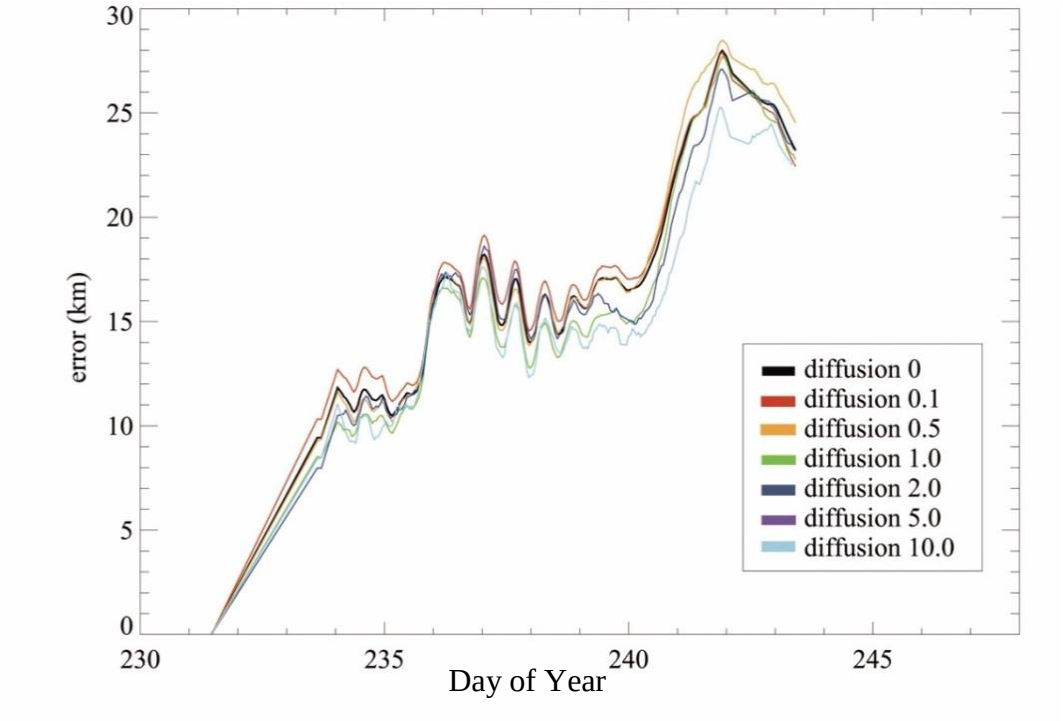

Figure 14. PTRAJ distance error (for drifter 1) for different horizontal diffusion values (shown by color) in August 2015.

To further explore the impact of diffusion effects, the errors were averaged for the period of observations and across three drifters (Figure 15).

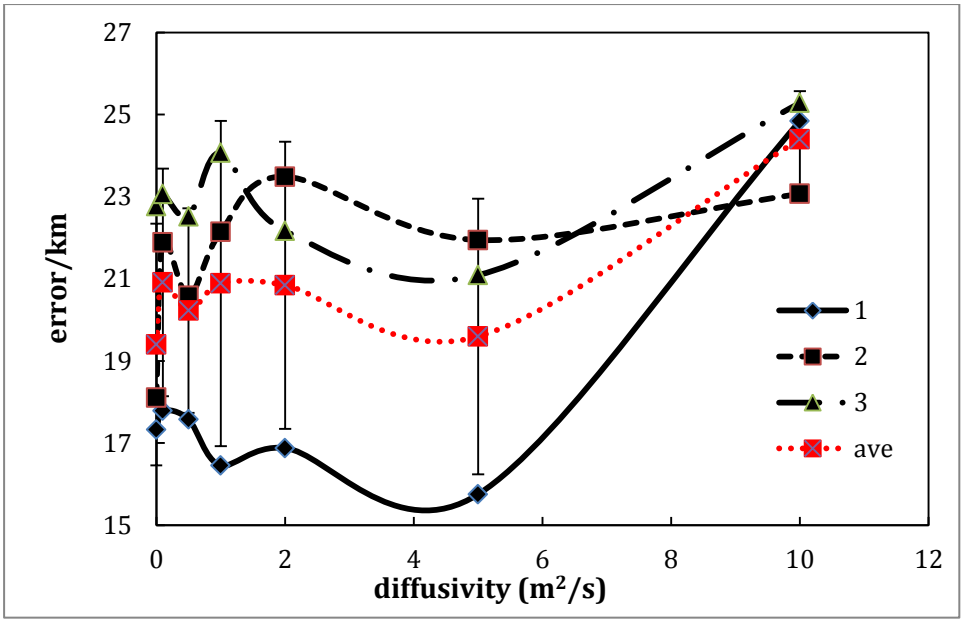

Figure 15. Average distance error for different horizontal diffusion values. Numbers represent individual drifters, and "ave: indicates an average error across three drifters.

When the PTRAJ model was run with zero horizontal diffusion; the averaged separation distance error was around 19.4 km (Fig. 15). Simulations conducted with different horizontal diffusion coefficients impacted the accuracy of model results only slightly for values in the range of 0-5.0 m^2/s since the error varied between 19.4 and 21.0 km. At the same time, the error grew to 24.4 km when the diffusion coefficient was increased to 10 m^2/s.

3. Circulation patterns produced by winds of various directions

Two important urban centers with water intakes in the western basin of Lake Erie may be adversely impacted by algae-rich (and potentially toxic) water from the Maumee River and Maumee Bay: Toledo, OH, and Monroe, MI. Toledo water intake is located to the east of Maumee Bay along the southern shoreline, while the Monroe water intake is located to the north-east of Maumee Bay (Figure 16).

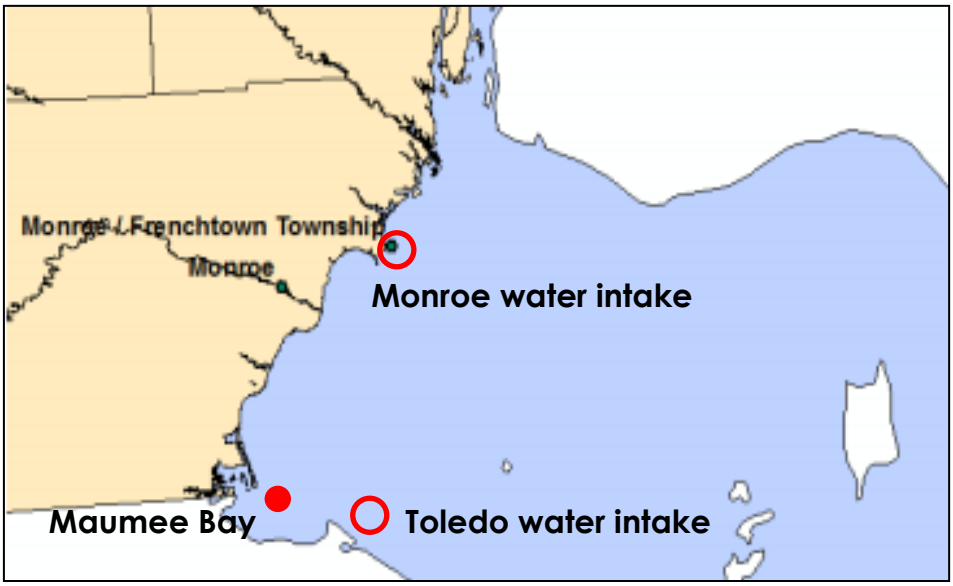

Figure 16. Location of Toledo and Monroe water intakes.[9]

As the 2014 Toledo water crisis demonstrated, the water from Maumee Bay can reach its water intake in a matter of days when appropriate conditions form; i.e., strong eastward currents driven by sustained NW winds. It is not clear though if similar transport can occur and impact the Toledo intake under different wind conditions or what kind of wind conditions can potentially impact Monroe intake (which is typically in the Detroit River water zone of influence). Therefore, to better

[9] The map source is Current State of Harmful Algal Bloom Impacts on Michigan Drinking Water Supplies, Sep. 2014. Available at: https://www.michigan.gov/documents/deq/deq-odwma-water-cdw-HAB_Impacts_467739_7.pdf

understand conditions when water can be transported from Maumee Bay to the coastlines of the Toledo or Monroe intakes, we conducted a joint analysis of 2014 to 2016 wind data and modeled circulation.

We used wind data from NOAA NDBC records for 2014 to 2016, using the same stations described in section 1.1. Circulation patterns in the western basin of Lake Erie were obtained from historic FVCOM simulations produced by the Great Lakes Coastal Forecasting System (Anderson et al. 2015) with INTERP forcing (coastal circulation in Toledo-Monroe area was qualitatively similar in INTERP and HRRR cases). Velocity vectors were averaged over water depth (since HABs can spread through water column) and in time to produce daily values.

Firstly, sustained strong wind events for eight wind directions (N-NE-E…NW) were identified during the summers of 2014, 2015 and 2016. Then, depth-average circulation was plotted for identified wind episodes. By combining both results, we were able to identify wind directions that result in strong currents impacting either Monroe or Toledo water intake. Analysis showed that there was a sufficient number of wind events in 2014 and 2015 alone to cover all eight wind directions (Table 3) and therefore remaining 2015 and 2016 events are not shown. As an example, Figure 17 showed hourly time-series of wind vector (along with speed and direction) during the SW and NW wind cases on August 30 and July 29, 2014, respectively. These examples were selected because SW winds are the prevailing winds over Lake Erie (Farhadzadeh, Hashemi, and Neill 2017) while a NW wind caused Toledo water crisis in 2014. Remaining wind cases were shown in Appendix C.

The corresponding circulations under SW and NW winds were shown in Figure 18. The model predicts strong currents directed from the Maumee Bay towards Monroe under SW winds, and strong currents from Maumee Bay towards Toledo under NW winds. Remaining six coastal circulation cases were shown in Appendix D. Analysis of all eight wind cases (Table 3) revealed under which circumstances nutrient-rich water with a higher concentration of HABs as well as the potentially high concentration of microcystins may contaminate water at Toledo and Monroe water treatment plant intakes, threatening water intake and local water consumption.

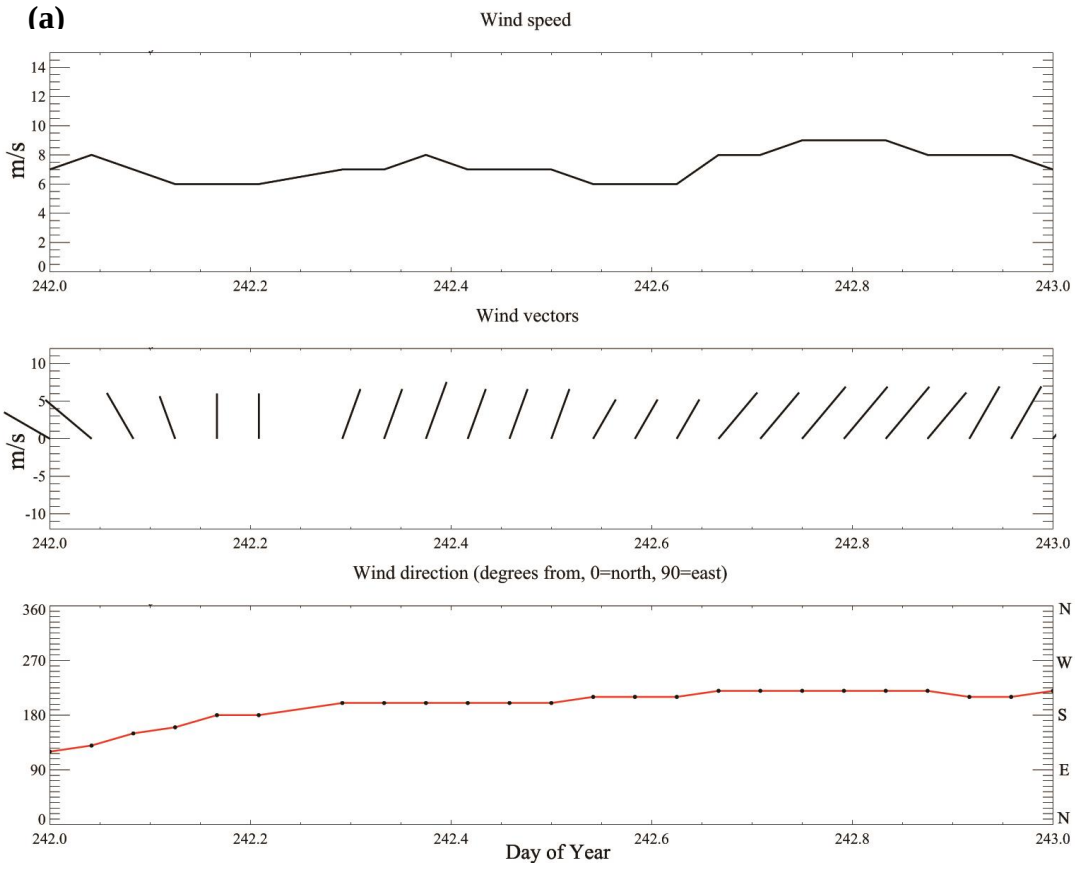

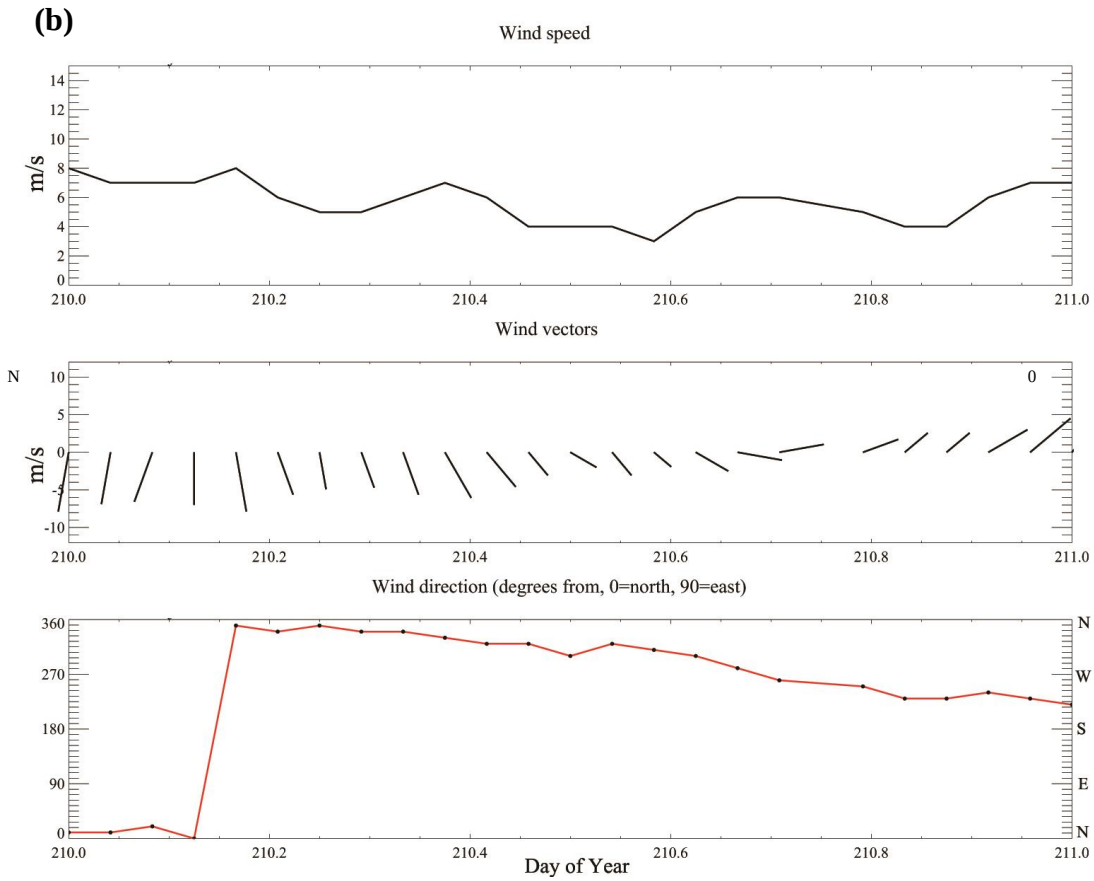

Figure 17. Observed hourly wind speed, wind vector and wind direction at buoy 45005 for SW wind (August 30, 2014, subplot "a") and NW wind (July 29, 2014, subplot "b") episodes.

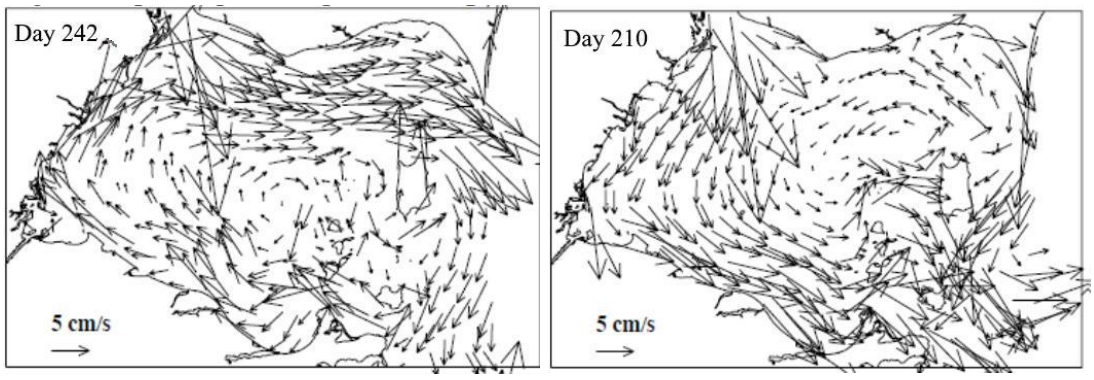

Figure 18. Modeled depth-average circulation (INTERP forcing) driven by SW (left) and NW (right) winds on August 30 and July 29, 2014 respectively. Winds are shown in Figure 17.

Table 3. Wind direction during select wind events and intakes impacted (T-Toledo, M-Monroe).

	Wind Event								
Year	Date	NE	N	NW	W	SW	S	SE	E
2014	Jul 24		T						
	Jul 28/29			T					
	Aug 10								X
	Aug 24							M	
	Aug 30					M			
2015	Jul 15	T							
	Jul 30				T				
	Aug 19						M		

In particular, we found that sustained NE-N-NW-W winds will transport water eastward from the Maumee Bay to the Toledo water intake (potentially repeating conditions of 2014 crisis - if strong bloom exists in Maumee Bay). On the contrary, winds of opposite directions (SE-S-SW) can impact conditions at Monroe water intake because they will transport water north-eastward: from the Maumee Bay to Monroe.

Discussion

Impact of circulation on bloom development

Although mean (12-day average) circulation looked rather similar in most areas of western basin in both INTERP and HRRR runs, we found significant difference south and west of the South Bass Island. In the HRRR model, the water flowed into the Western Basin from the Central Basin while in INTERP case water moved in opposite direction. Interestingly enough, satellite imagery showed disappearance of HABs near the South Bass Island area near the end of August. A plausible explanation is that freshwater with a lower concentration of HABs from the Central Basin flushed and displaced the blooms in this area which would be consistent with HRRR circulation pattern but not INTERP. Model skill assessment in the northern part of western basin did not reveal an advantage of one type of forcing over the other, however, based on the satellite data in the southern area we may conclude that HRRR forcing produced more accurate circulation in western basin overall.

Impact of horizontal diffusivity on PTRAJ results

FVCOM results with different driving forces, i.e., INTERP and HRRR, showed they both underestimated current speed. The PTRAJ model also showed slower movement of virtual drifters as compared with observations, in line with slower currents in FVCOM. Tests with increased horizontal diffusivity revealed that the distance errors were rather weakly impacted by diffusivity. We, therefore, conclude that the cause of discrepancy lied in the underestimation of surface currents driving PTRAJ.

Movement of Drifter and Blooms: Surface versus 3D drift

Observations showed that drifters moved faster than the bloom leading edge and this difference (in addition to biological processes and mixing of bloom waters with colder and nutrient poor waters of Detroit River and central basin where blooms rarely propagate, unlike drifters) may be also due to the fact that while drifters only floated on the surface, HABs movement is three-dimensional and is impacted by currents at different depths. Indeed, model results showed that currents at depth are substantially weaker than the surface currents. In addition, wind-driven vertical mixing, buoyancy, and migration are also important factors of HAB dynamics. E.g., when wind decreases, higher surface bloom concentrations are observed due to buoyancy regulation by *Microcystis* (Wynne et al. 2010). Hunter et al. (2008) proposed a threshold of wind speed at 4 m/s, below which is a nonturbulent mixing and increased water column stability (Hunter et al. 2008). Yamazaki & Kamykowski (1991) showed that for motile phytoplankton, the wind energy required to alter the diel vertical migration was directly linked to the buoyancy and the capability to use flagella and cilia to move (Yamazaki and Kamykowski 1991). According to Niu & Xia's study on wave climatology of Lake Erie, the near shore of the Western Basin is most likely to be affected by the wave-induced orbital oscillations (Niu and Xia 2016).

Model limitations

There are some limitations in this study that can potentially be improved in the future. For example, accuracy of model results is impacted not only by meteorological forcing but also limitations of model physics. Niu & Xia's recent study on Lake Erie hydrodynamics using a high-resolution wave-current coupled model system suggested that radiation stress plays important role in generating wave-induced current in

nearshore regions, especially in the shallow Western Basin. Overall, the wave-induced surface and radiation stresses are both important in Lake Erie Hydrodynamics for both the seasonal-mean and episodic scales (Niu and Xia 2017). The version of FVCOM we used did not have this wave-current interaction component and that will be desirable to consider in future research. Another area for improvement is to consider the Stokes drift, which is driven by the local wind and is in the direction of the wind (Clarke and Van Gorder 2018). Stokes drift (which is most pronounced in the surface layer) impacts drifter movement so the lack of it can potentially explain underestimation of modeled surface current speed.

Conclusions

This study used drifter observations and hydrodynamic modeling (FVCOM and Lagrangian particle model PTRAJ) to analyze physical processes and model uncertainty in the western basin of Lake Erie. Drifter data were used for model validation and results indicate the directions for model improvement. Currents produced by strong wind events were selected and analyzed for 2014, 2015 and 2016. We identified wind directions when water can be quickly transported from the Maumee River to Monroe or Toledo water intakes (i.e., SE-S-SW and NE-N-NW-W, respectively). Those wind directions are hence of particular concern for water intake management when the upcoming water contains high concentration of HABs. Because when the water moves into those directions, HABs may be transported, too: this may contaminate the water intake and influence safety of local drinking water. HABs dynamics are impacted by multiple factors such as wind, currents, temperature and nutrients. Despite the need to improve model accuracy further, hydrodynamic modeling is a powerful tool in predicting HABs and relevant management applications.

Recommendations for future studies

Improvements in hydrodynamic modeling of Lake Erie are essential in understanding the movement of water and transport of HABs and decision making to improve management of lakes. To make better predictions, more accurate advection is needed. On the other hand, vertical diffusivity and mixing need also be further researched to have better model prediction of the vertical distribution of phytoplankton. In addition, some model limitations need to be addressed, such as inclusion of radiation stress and Stokes drift. Finally, while we identified some critical wind directions for water intake impacts this topic needs to be researched more in the future to improve HAB forecasts, e.g. use satellite and weekly monitoring data to confirm model predicted movement of HABs during strong wind events.

Bibliography

Anderson, Eric J., Adam J. Bechle, Chin H. Wu, David J. Schwab, Greg E. Mann, and Kirk A. Lombardy. 2015. 'Reconstruction of a meteotsunami in Lake Erie on 27 May 2012: Roles of atmospheric conditions on hydrodynamic response in enclosed basins', *Journal of Geophysical Research: Oceans*, 120: 8020-38.

Anderson, Eric J., David J. Schwab, and Gregory A. Lang. 2010. 'Real-Time Hydraulic and Hydrodynamic Model of the St. Clair River, Lake St. Clair, Detroit River System', *Journal of Hydraulic Engineering*, 136: 507-18.

Beletsky, D., N. Hawley, and Y. R. Rao. 2013a. 'Modeling summer circulation and thermal structure of Lake Erie', *J. Geophys Res: Oceans*, 118: 6238.

Bolsenga, Stanley J, and Charles E Herdendorf. 1993. *Lake Erie and Lake St. Clair Handbook* (Wayne State University Press).

Bridgeman, Thomas B., Justin D. Chaffin, Douglas D. Kane, Joseph D. Conroy, Sarah E. Panek, and Patricia M. Armenio. 2012. 'From River to Lake: Phosphorus partitioning and algal community compositional changes in Western Lake Erie', *Journal of Great Lakes Research*, 38: 90-97.

Carrick, Hunter J., Jessica B. Moon, and Barrett F. Gaylord. 2005. 'Phytoplankton Dynamics and Hypoxia in Lake Erie: A Hypothesis Concerning Benthic-pelagic Coupling in the Central Basin', *Journal of Great Lakes Research*, 31: 111-24.

Chen, Changsheng. 2012. *An Unstructured-grid, Finite-volume Community Ocean Model: FVCOM User Manual* (Sea Grant College Program, Massachusetts Institute of Technology).

Chen, Changsheng, Hedong Liu, and Robert C Beardsley. 2003. 'An unstructured grid, finite-volume, three-dimensional, primitive equations ocean model: application to coastal ocean and estuaries', *Journal of atmospheric and oceanic technology*, 20: 159-86.

Clarke, Allan J, and Stephen Van Gorder. 2018. 'The Relationship of Near‐Surface Flow, Stokes Drift and the Wind Stress', *Journal of Geophysical Research: Oceans*, 123: 4680-92.

Farhadzadeh, Ali, M. Reza Hashemi, and Simon Neill. 2017. 'Characterizing the Great Lakes hydrokinetic renewable energy resource: Lake Erie wave, surge and seiche characteristics', *Energy*, 128: 661-75.

Fitzsimmons, Emma G. 2014. 'Tap Water Ban for Toledo Residents', *the New York Times*, Aug 3.

Gilbert, CS, WC Gentleman, CL Johnson, C DiBacco, JM Pringle, and C Chen. 2010. 'Modelling dispersal of sea scallop (Placopecten magellanicus) larvae on Georges Bank: The influence of depth-distribution, planktonic duration and spawning seasonality', *Progress in Oceanography*, 87: 37-48.

Hawley, Nathan, Thomas H Johengen, Yerubandi R Rao, Steven A Ruberg, Dmitry Beletsky, Stuart A Ludsin, Brian J Eadie, David J Schwab, Thomas E Croley, and Stephen B Brandt. 2006. 'Lake Erie hypoxia prompts Canada-US study', *Eos*, 87: 313-24.

Henry, Tom. 2014. 'Toledo seeks return to normalcy after do not drink water advisory lifted', *Toledo Blade*, Aug. 5.

Hunter, P. D., A. N. Tyler, N. J. Willby, and D. J. Gilvear. 2008. 'The spatial dynamics of vertical migration by Microcystis aeruginosa in a eutrophic

shallow lake: A case study using high spatial resolution time-series airborne remote sensing', *Limnology and Oceanography*, 53: 2391-406.

Michalak, A. M., E. J. Anderson, D. Beletsky, S. Boland, N. S. Bosch, T. B. Bridgeman, J. D. Chaffin, K. Cho, R. Confesor, I. Daloğlu, J. V. DePinto, M. A. Evans, G. L. Fahnenstiel, L. He, J. C. Ho, L. Jenkins, T. H. Johengen, K. C. Kuo, E. LaPorte, X. Liu, M. R. McWilliams, M. R. Moore, D. J. Posselt, R. P. Richards, D. Scavia, A. L. Steiner, E. Verhamme, D. M. Wright, and M. A. Zagorski. 2013. 'Record-setting algal bloom in Lake Erie caused by agricultural and meteorological trends consistent with expected future conditions', *Proc. Natl. Acad. Sci. U. S. A.*, 110: 6448.

Niu, Qianru, and Meng Xia. 2016. 'Wave climatology of Lake Erie based on an unstructured-grid wave model', *Ocean Dynamics*, 66: 1271-84.

———. 2017. 'The role of wave‐current interaction in L ake E rie's seasonal and episodic dynamics', *Journal of Geophysical Research: Oceans*, 122: 7291-311.

Rowe, M. D., E. J. Anderson, T. T. Wynne, R. P. Stumpf, D. L. Fanslow, K. Kijanka, H. A. Vanderploeg, J. R. Strickler, and T. W. Davis. 2016. 'Vertical distribution of buoyant Microcystis blooms in a Lagrangian particle tracking model for short-term forecasts in Lake Erie', *Journal of Geophysical Research: Oceans*, 121: 5296-314.

Rucinski, Daniel K., Joseph V. DePinto, Donald Scavia, and Dmitry Beletsky. 2014. 'Modeling Lake Erie's hypoxia response to nutrient loads and physical variability', *Journal of Great Lakes Research*, 40, Supplement 3: 151-61.

Scavia, D., J. David Allan, K. K. Arend, S. Bartell, D. Beletsky, N. S. Bosch, S. B. Brandt, R. D. Briland, I. Daloğlu, J. V. DePinto, D. M. Dolan, M. A. Evans, T. M. Farmer, D. Goto, H. Han, T. O. Höök, R. Knight, S. A. Ludsin, D. Mason, A. M. Michalak, R. Peter Richards, J. J. Roberts, D. K. Rucinski, E. Rutherford, D. J. Schwab, T. M. Sesterhenn, H. Zhang, and Y. Zhou. 2014. 'Assessing and addressing the re-eutrophication of Lake Erie: Central basin hypoxia', *J. Great Lakes Res.*, 40: 226.

Schwab, David J. 1983. 'Numerical simulation of low-frequency current fluctuations in Lake Michigan', *Journal of physical oceanography*, 13: 2213-24.

Steffen, Morgan M., B. Shafer Belisle, Sue B. Watson, Gregory L. Boyer, and Steven W. Wilhelm. 2014. 'Status, causes and controls of cyanobacterial blooms in Lake Erie', *Journal of Great Lakes Research*, 40: 215-25.

Strasserf, Reto J, Alaka Srivastava, and Govindjee. 1995. 'Polyphasic chlorophyll a fluorescence transient in plants and cyanobacteria', *Photochemistry and photobiology*, 61: 32-42.

Wynne, Timothy T, Richard P Stumpf, Michelle C Tomlinson, Gary L Fahnenstiel, Julianne Dyble, David J Schwab, and Sonia Joseph Joshi. 2013. 'Evolution of a cyanobacterial bloom forecast system in western Lake Erie: Development and initial evaluation', *Journal of Great Lakes Research*, 39: 90-99.

Wynne, Timothy T, Richard P Stumpf, Michelle C Tomlinson, David J Schwab, Glen Y Watabayashi, and John D Christensen. 2011. 'Estimating cyanobacterial bloom transport by coupling remotely sensed imagery and a hydrodynamic model', *Ecological Applications*, 21: 2709-21.

Wynne, Timothy T., Richard P. Stumpf, Michelle C. Tomlinson, and Julianne Dyble. 2010. 'Characterizing a cyanobacterial bloom in Western Lake Erie using satellite imagery and meteorological data', *Limnology and Oceanography*, 55: 2025-36.

Yamazaki, Hidekatsu, and Daniel Kamykowski. 1991. 'The vertical trajectories of motile phytoplankton in a wind-mixed water column', *Deep Sea Research Part A. Oceanographic Research Papers,* 38: 219-41.

Appendices

Appendix A. GLERL HAB Bulletin[10]

HAB Bulletin 2014

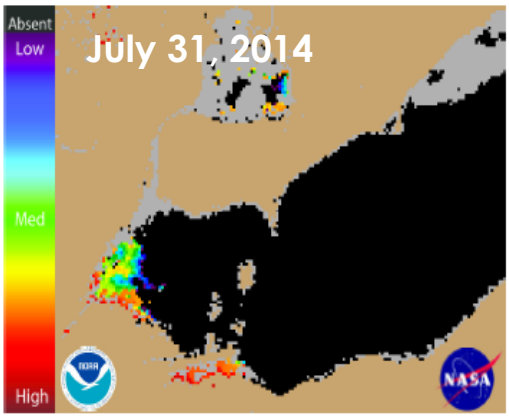

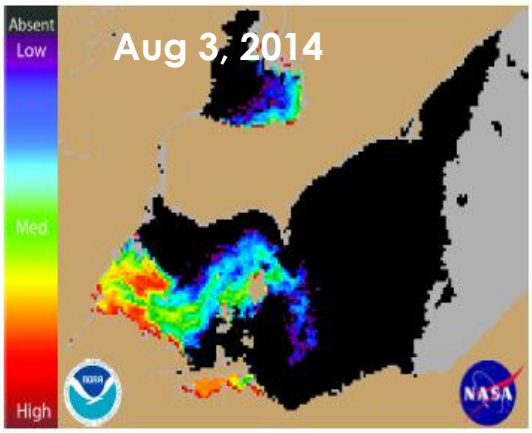

[10] HABs information from GLERL HAB Bulletin,

https://www.glerl.noaa.gov/res/HABs_and_Hypoxia/lakeErieHABArchive/

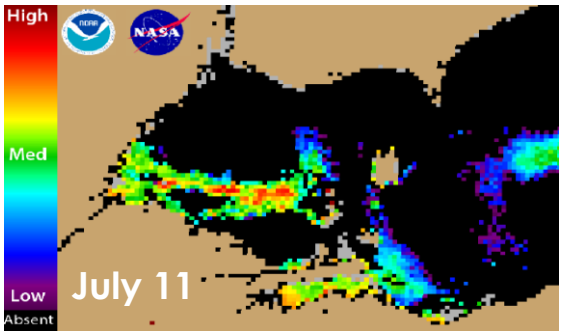
High
Med
Low
Absent
July 11

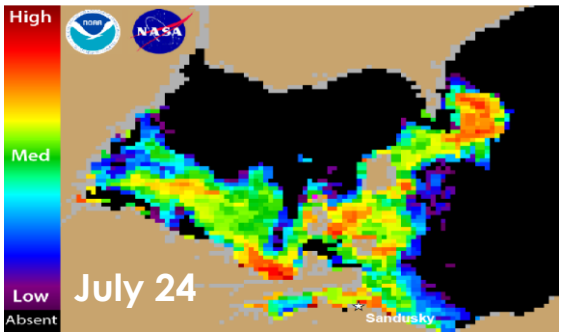
High
Med
Low
Absent
July 24
Sandusky

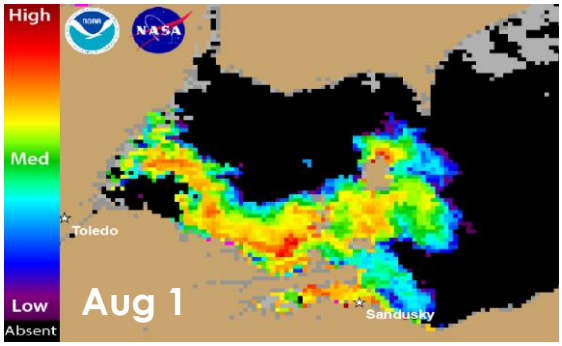
High
Med
Low
Absent
Toledo
Aug 1
Sandusky

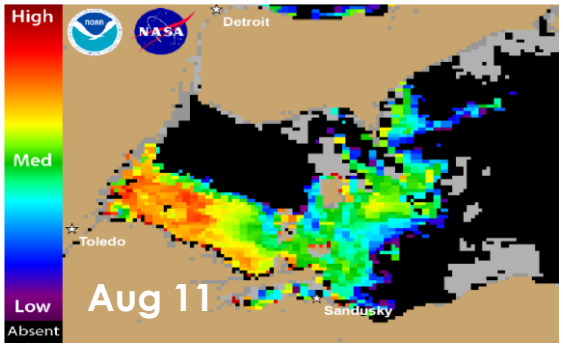
High
Med
Low
Absent
Detroit
Toledo
Aug 11
Sandusky

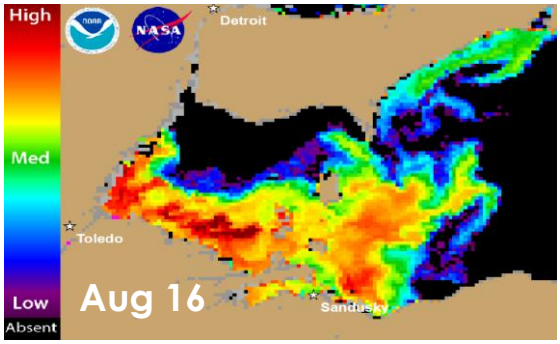
High
Med
Low
Absent
Detroit
Toledo
Aug 16
Sandusky

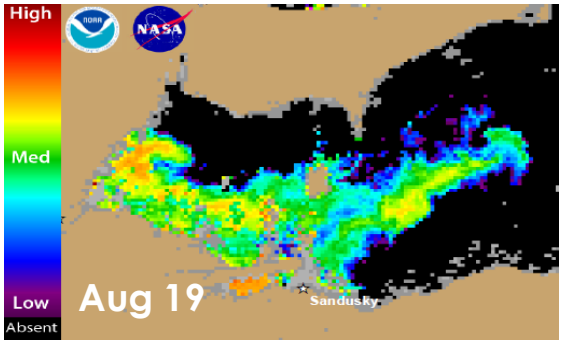
High
Med
Low
Absent
Aug 19
Sandusky

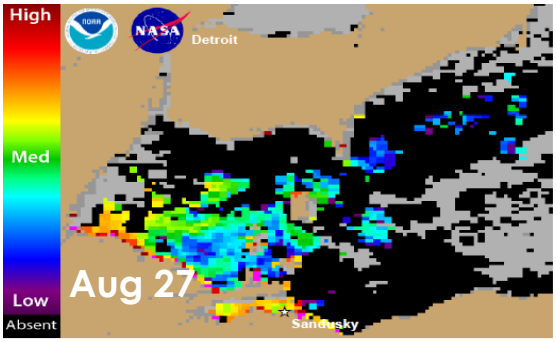
High
Med
Low
Absent
Detroit
Aug 27
Sandusky

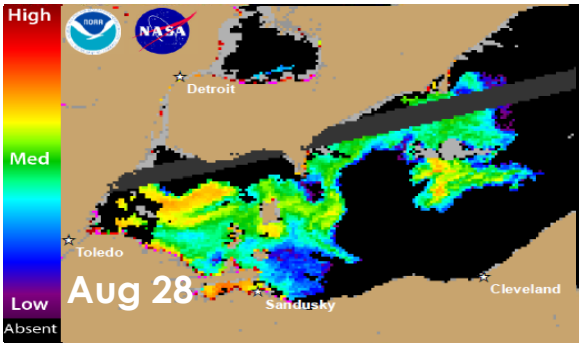
High
Med
Low
Absent
Detroit
Toledo
Aug 28
Sandusky
Cleveland

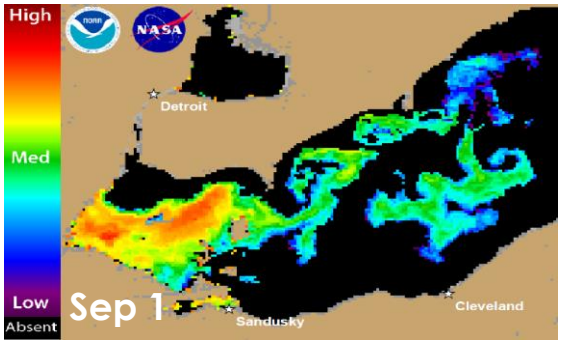
High
Med
Low
Absent
Detroit
Sep 1
Sandusky
Cleveland

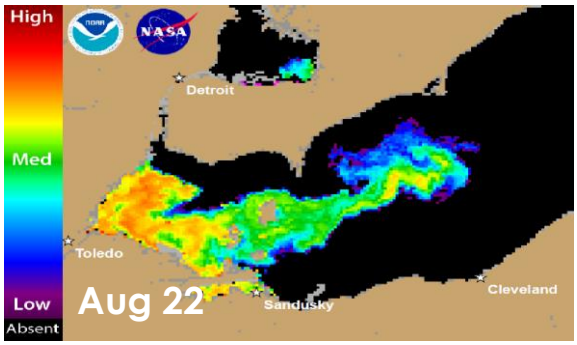
High
Med
Low
Absent
Detroit
Toledo
Aug 22
Sandusky
Cleveland

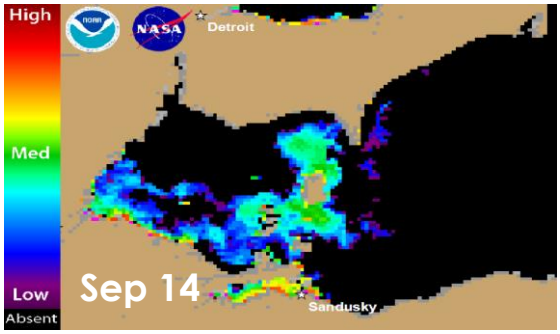
High
Med
Low
Absent
Detroit
Sep 14
Sandusky

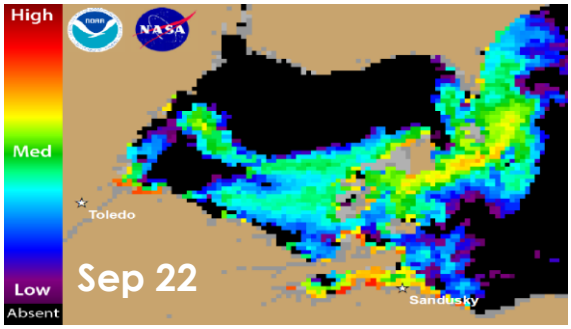
High
Med
Low
Absent
Toledo
Sep 22
Sandusky

Appendix B. Model Validation Results

i. Validation of velocities and speed

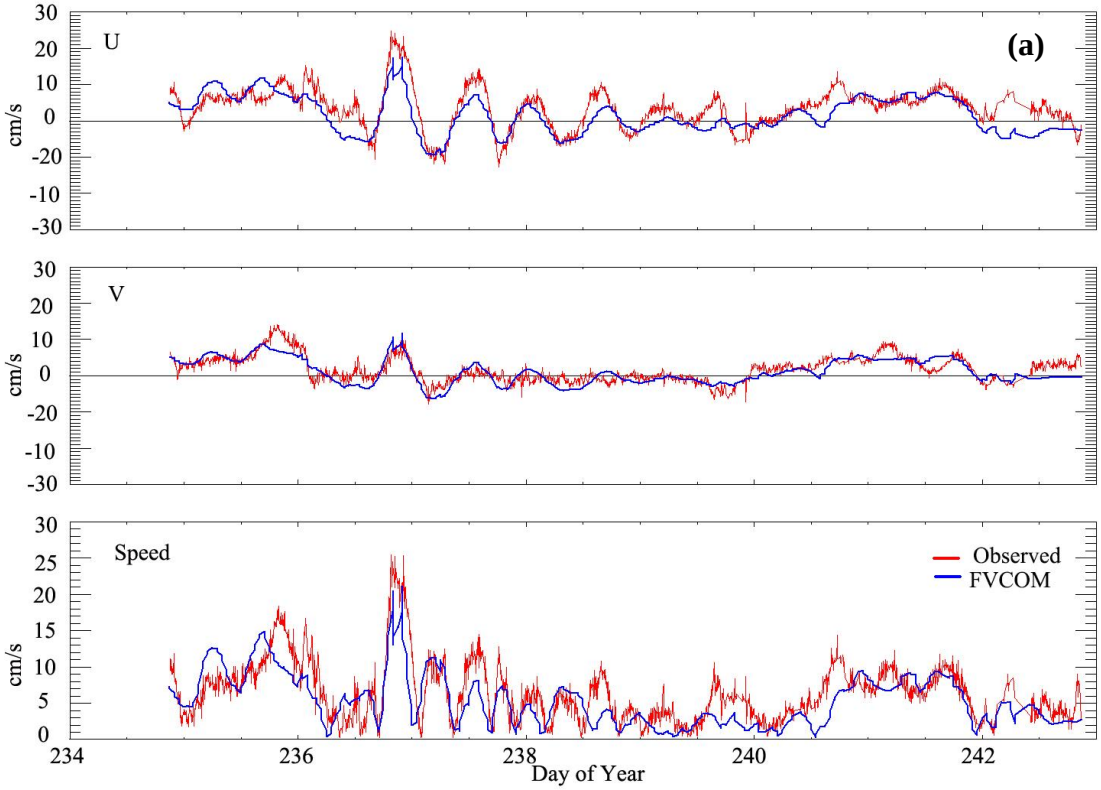

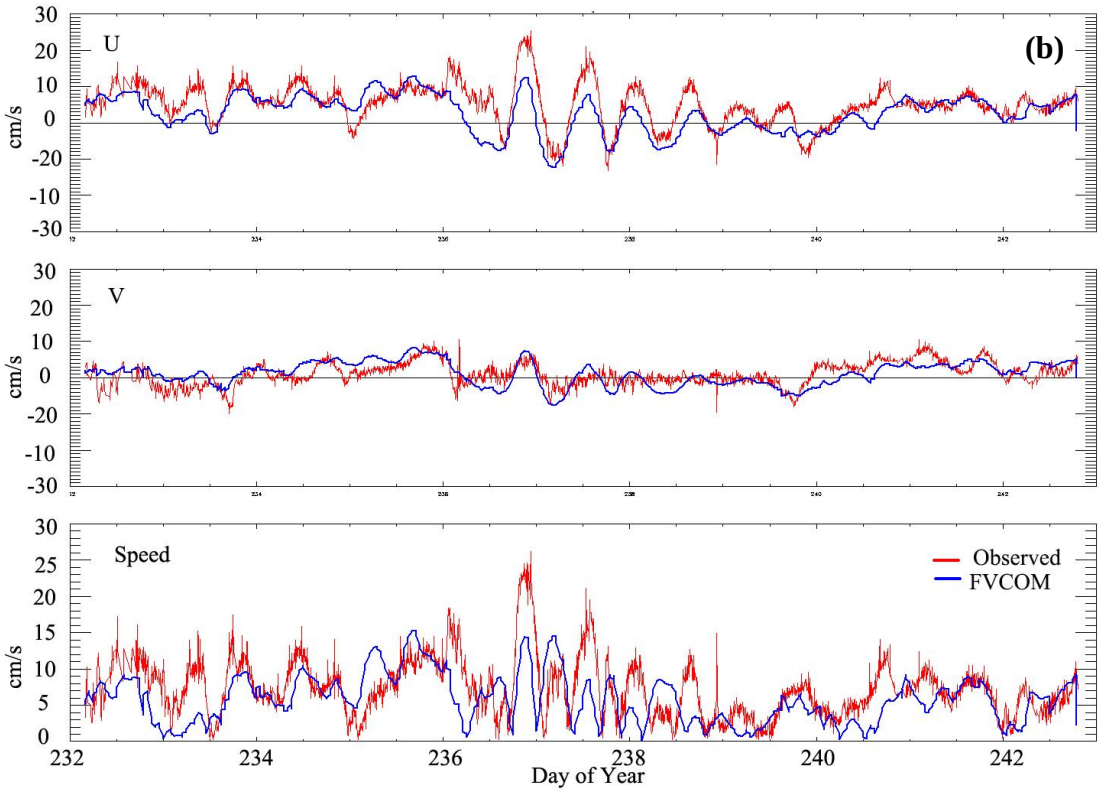
(b)
U
V
Speed
Observed
FVCOM
cm/s
Day of Year

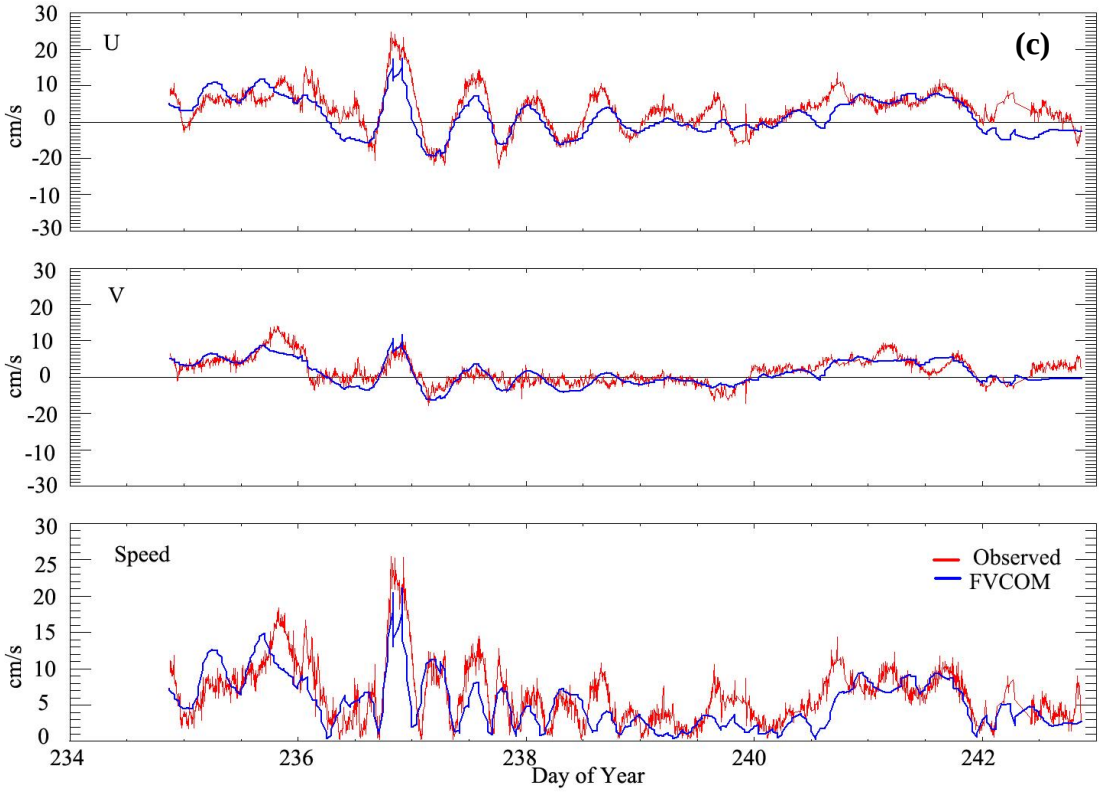
(c)
U
V
Speed
Observed
FVCOM
cm/s
Day of Year

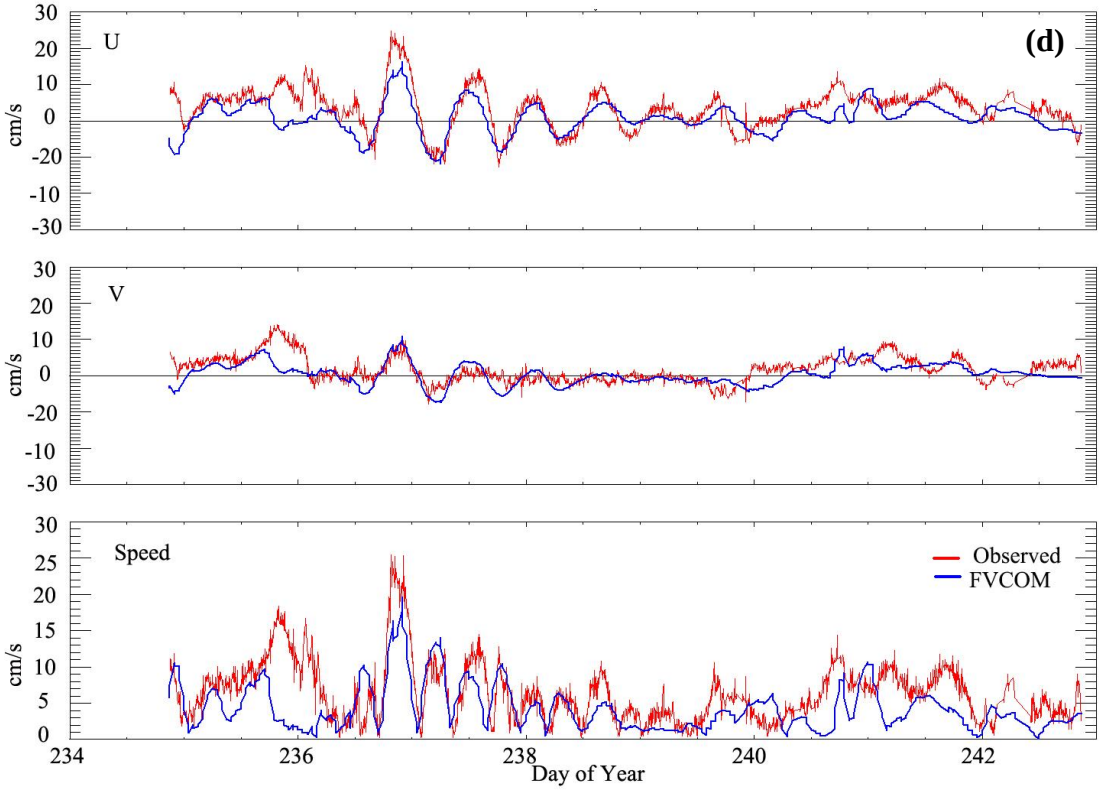
(d)
U
V
Speed
Observed
FVCOM
cm/s
Day of Year

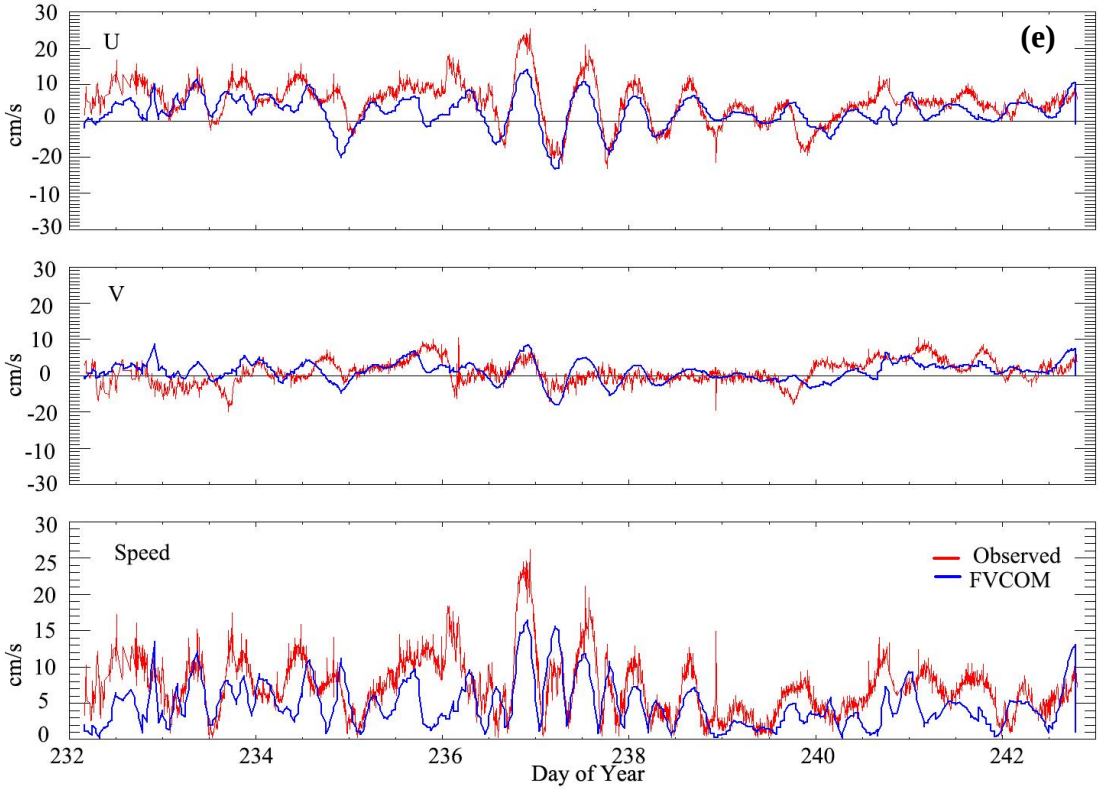
(e)
U
V
Speed
Observed
FVCOM
cm/s
Day of Year

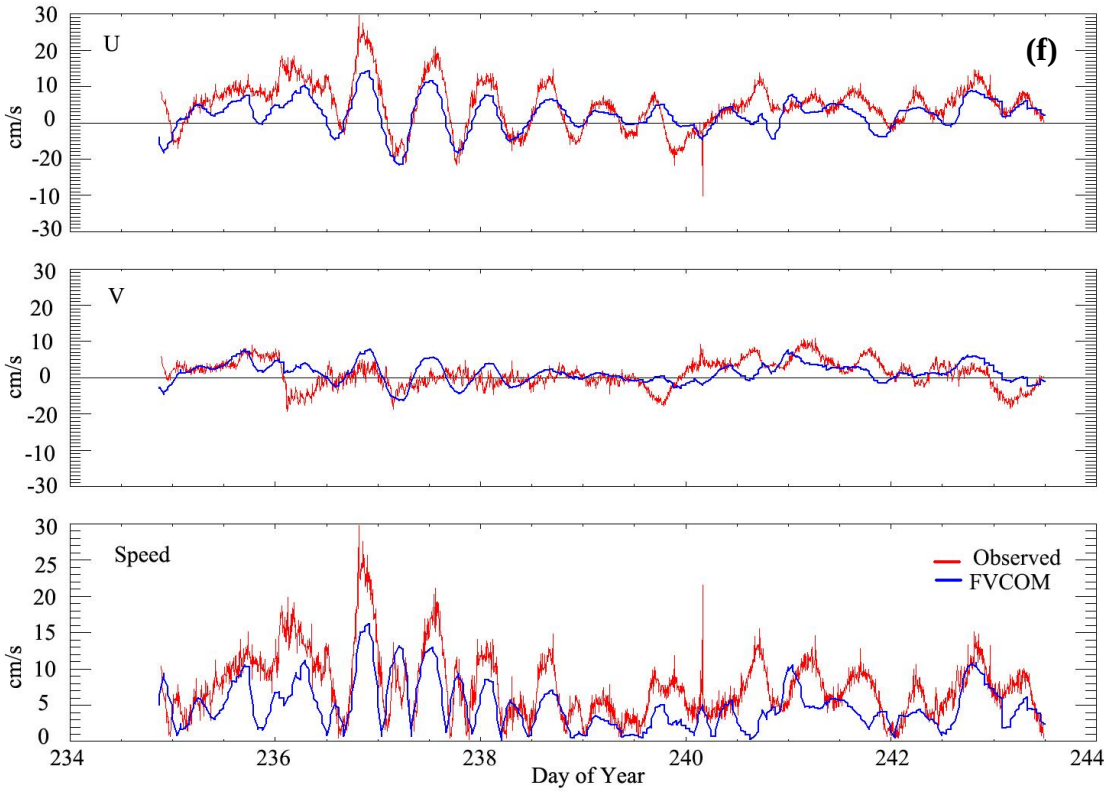

Figure B.1 Velocity and speed plot of drifter observation and model output.
(a) and (b), (c) and (d), and (e) and (f) correspond to the results of the three drifters, i.e., drifter 1, 2, and 3, respectively. (a), (c), and (e) uses INTERP model outputs and (b), (d), and (f) use HRRR model output.

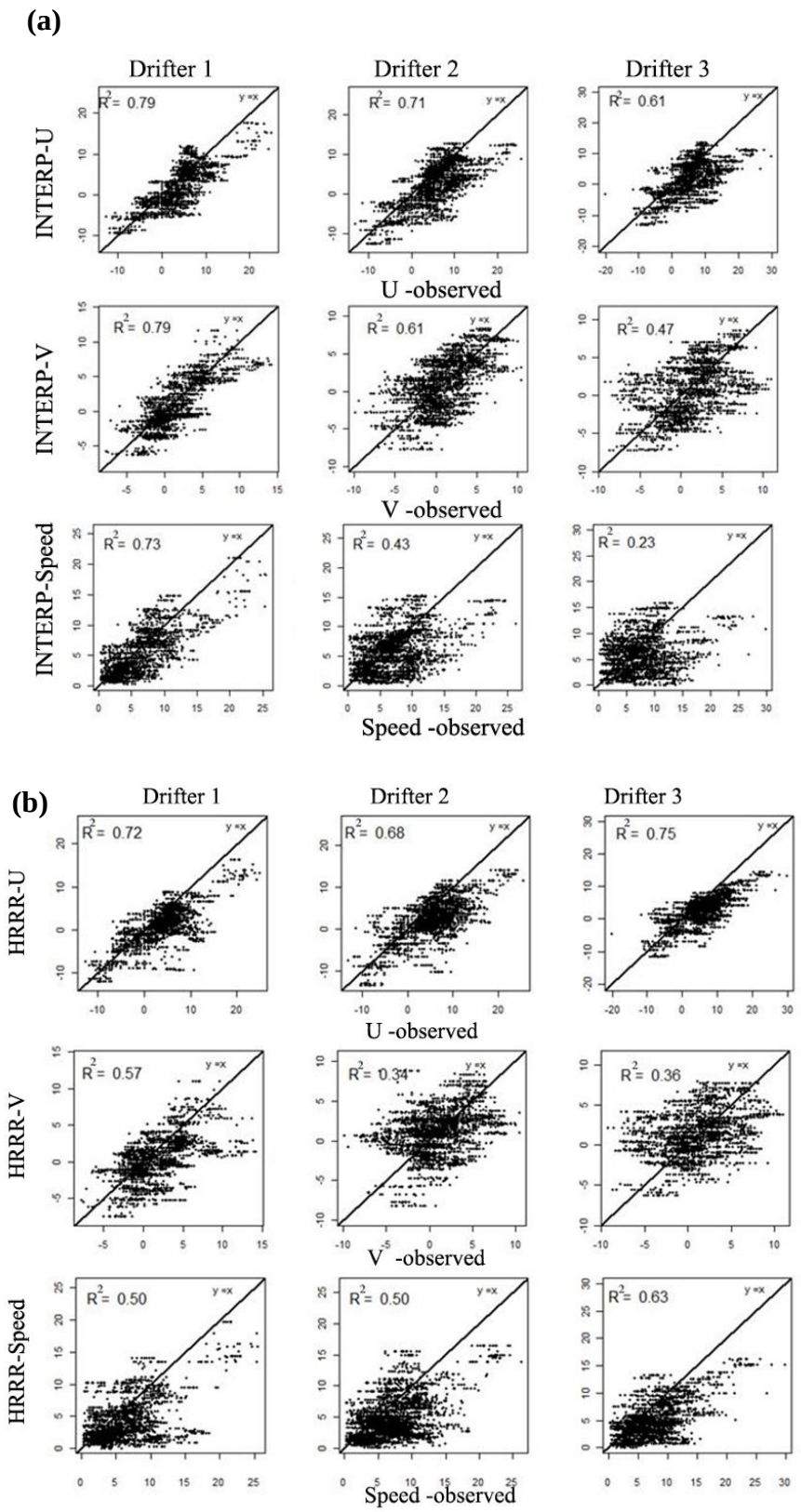

Figure B.2 Linear regressions of observations and model results for velocity components U (top row), V (middle row) and current speed (bottom row). Observed velocities (cm/s) are plotted along x-axis and model results along y-axis. Subplot (a) uses the output from the INTERP case and subplot (b) uses the output from the HRRR case. Columns represent individual drifters.

ii. Validation of water level

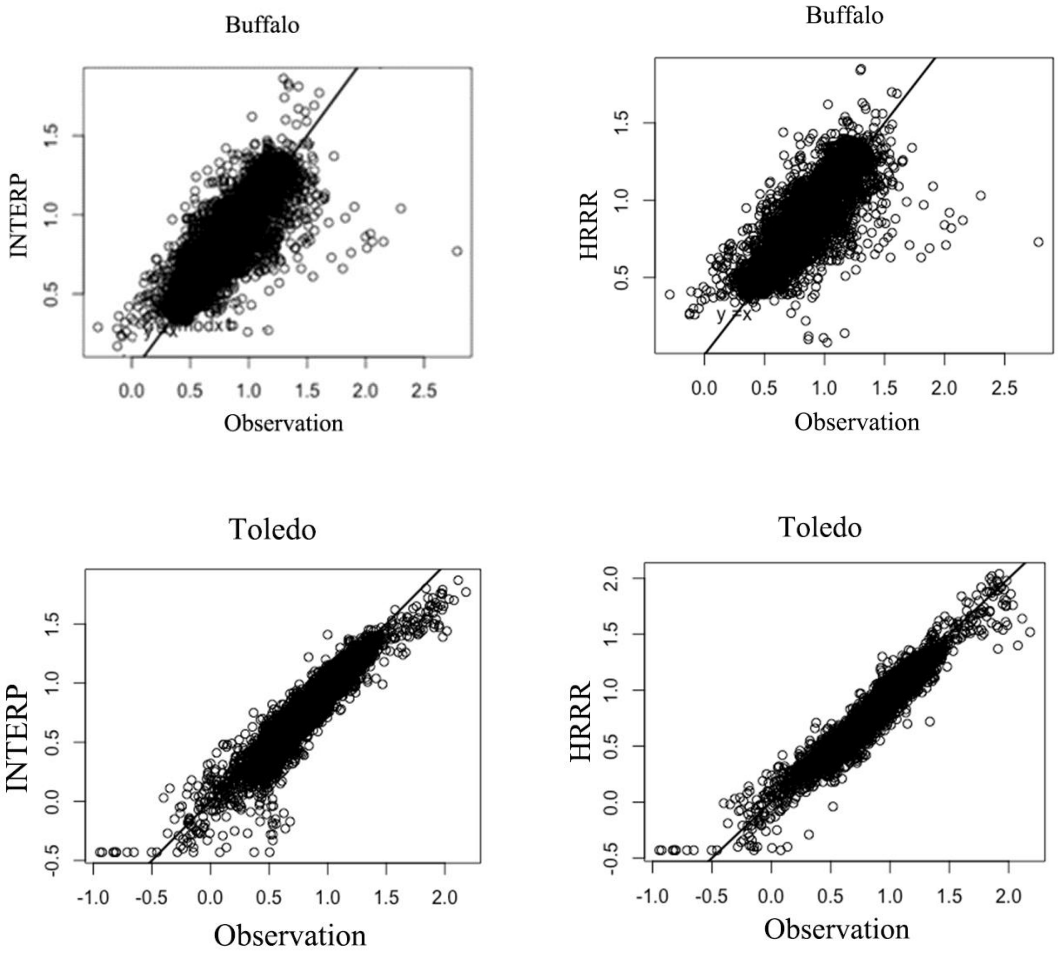

Figure B.3 Linear regression of water level: observations versus model. Results for Buffalo are shown in the top row, results for Toledo in the bottom row. Left column represents INTERP case and right column represents HRRR case.

Appendix C. Wind Speed and Direction during Selected Wind Episodes

North Wind (N)

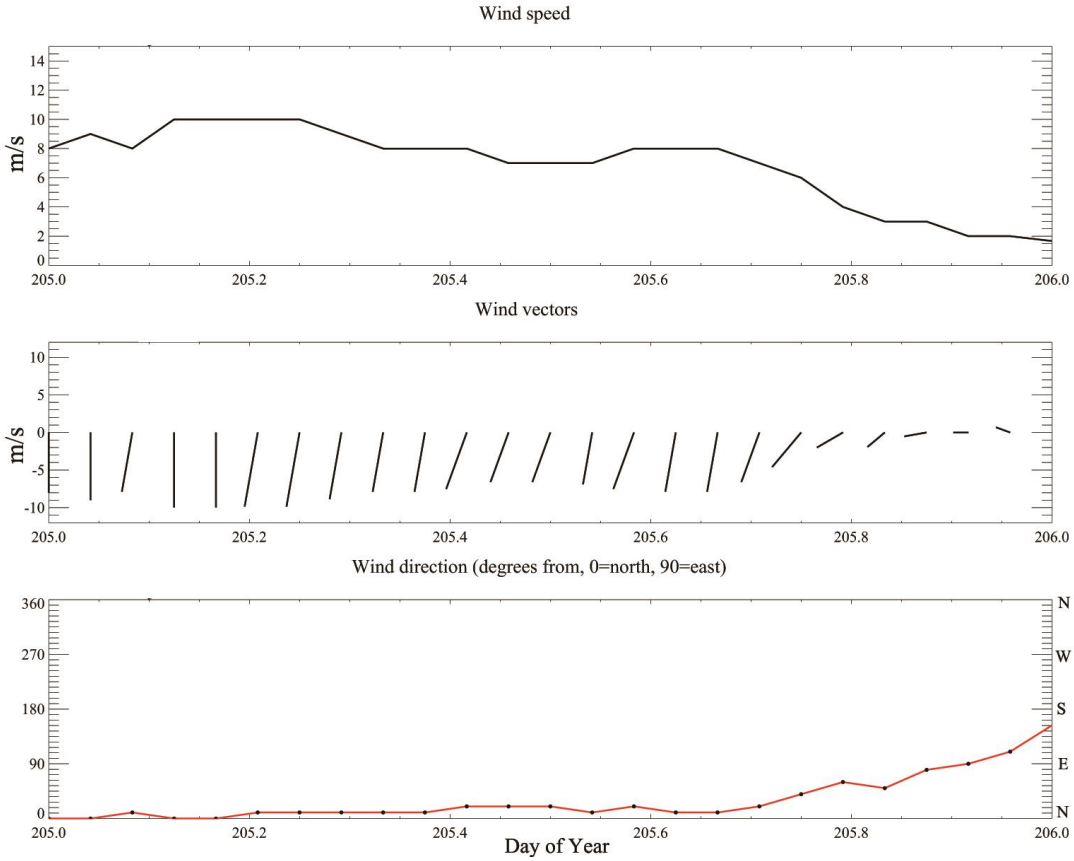

Observed hourly wind on July 24, 2015 (Day 205), buoy 45005

Northwest wind (NW)

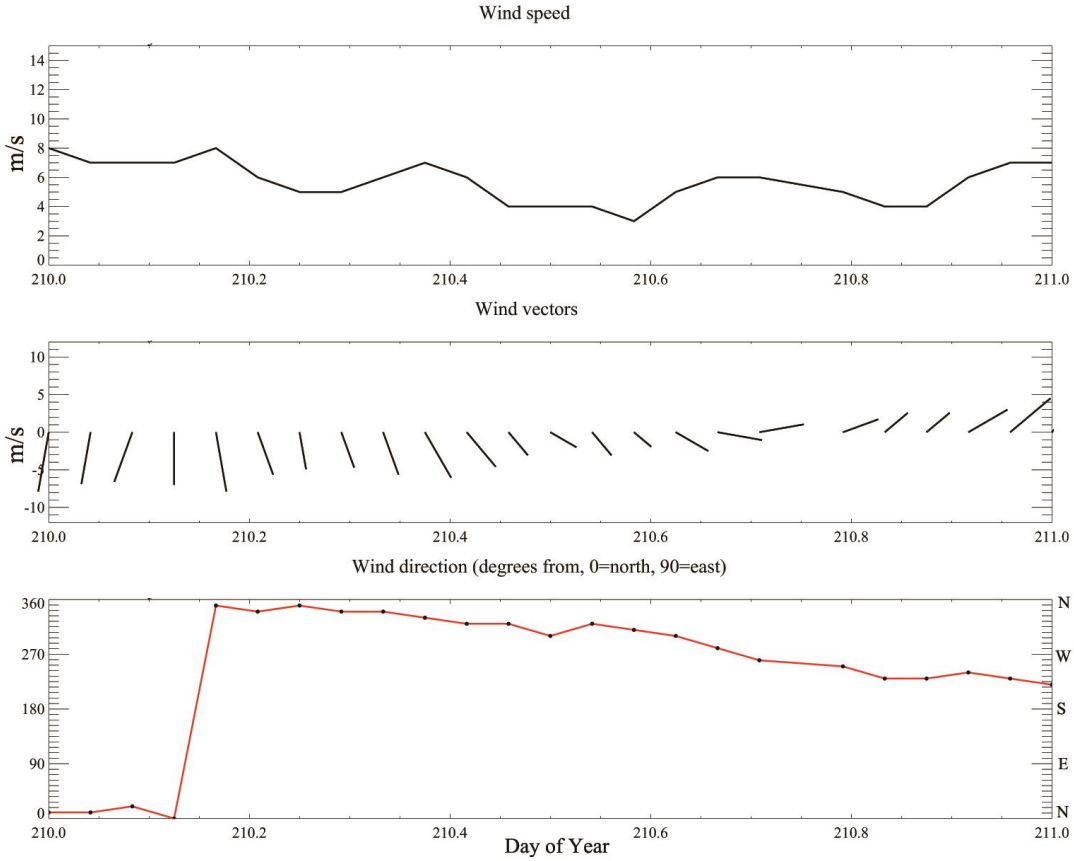

Observed hourly wind on July 29, 2014 (Day 210), buoy 45005

West wind (W)

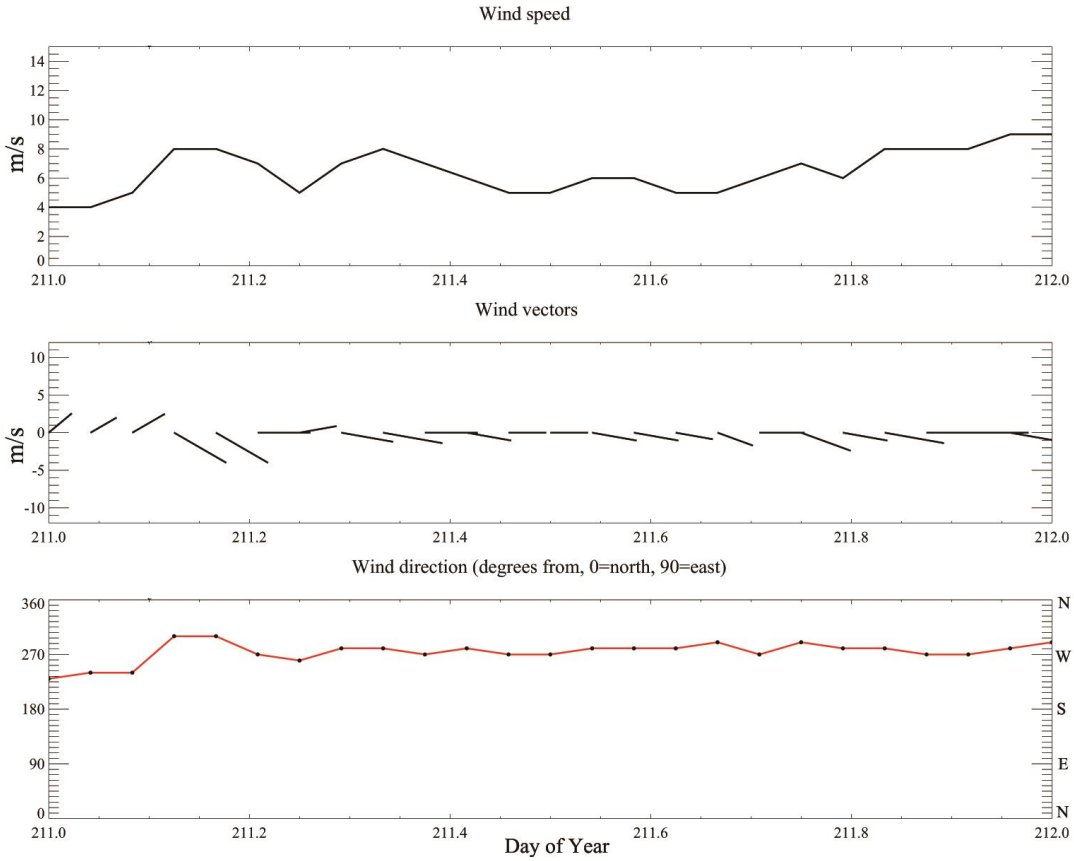

Observed hourly wind on July 30, 2015 (Day 211), buoy 45165

Southwest wind (SW)

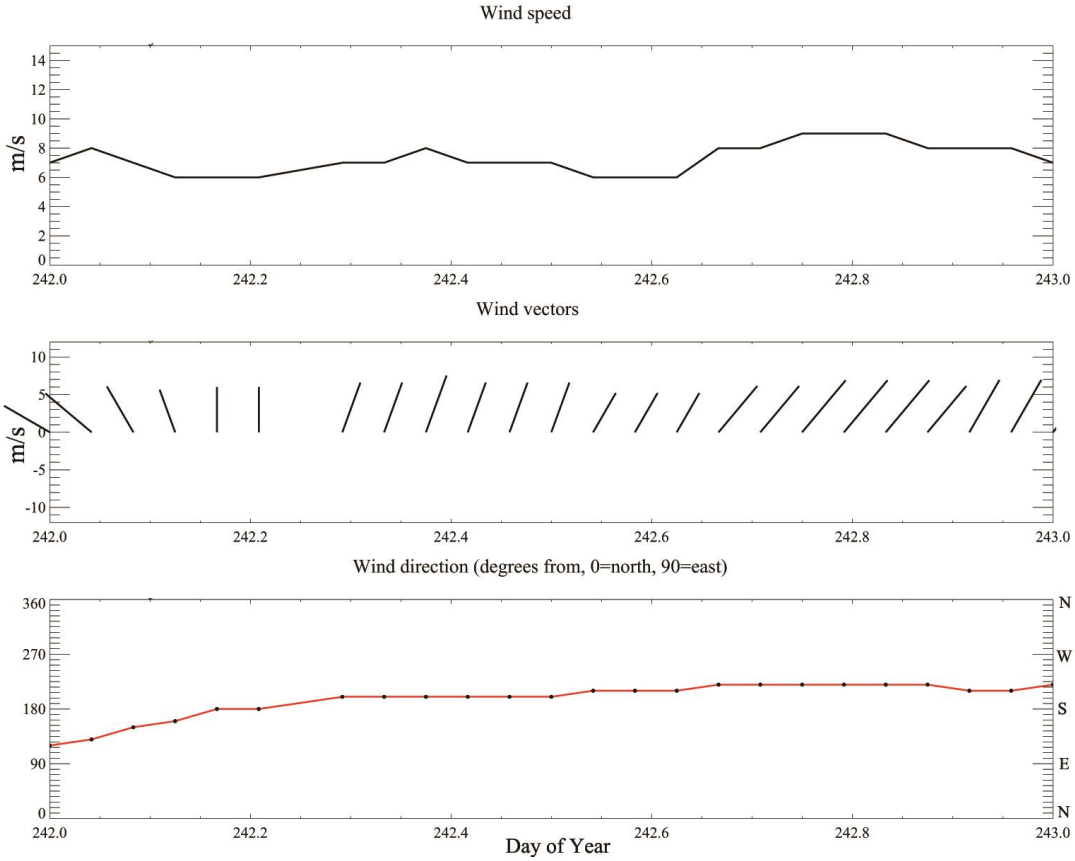

Observed hourly wind on August 30, 2014 (Day 242), buoy 45165

South wind (S)

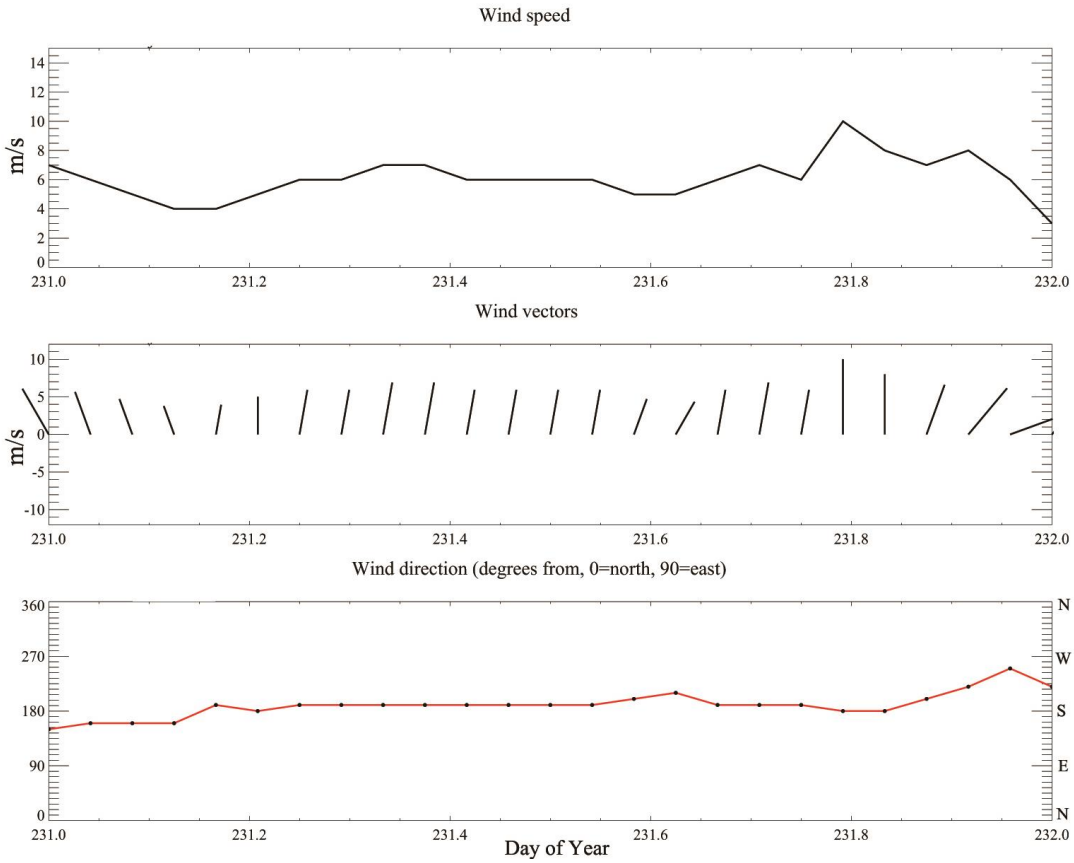

Observed hourly wind on August 19, 2015 (Day 231), buoy 45165

Southeast wind (SE)

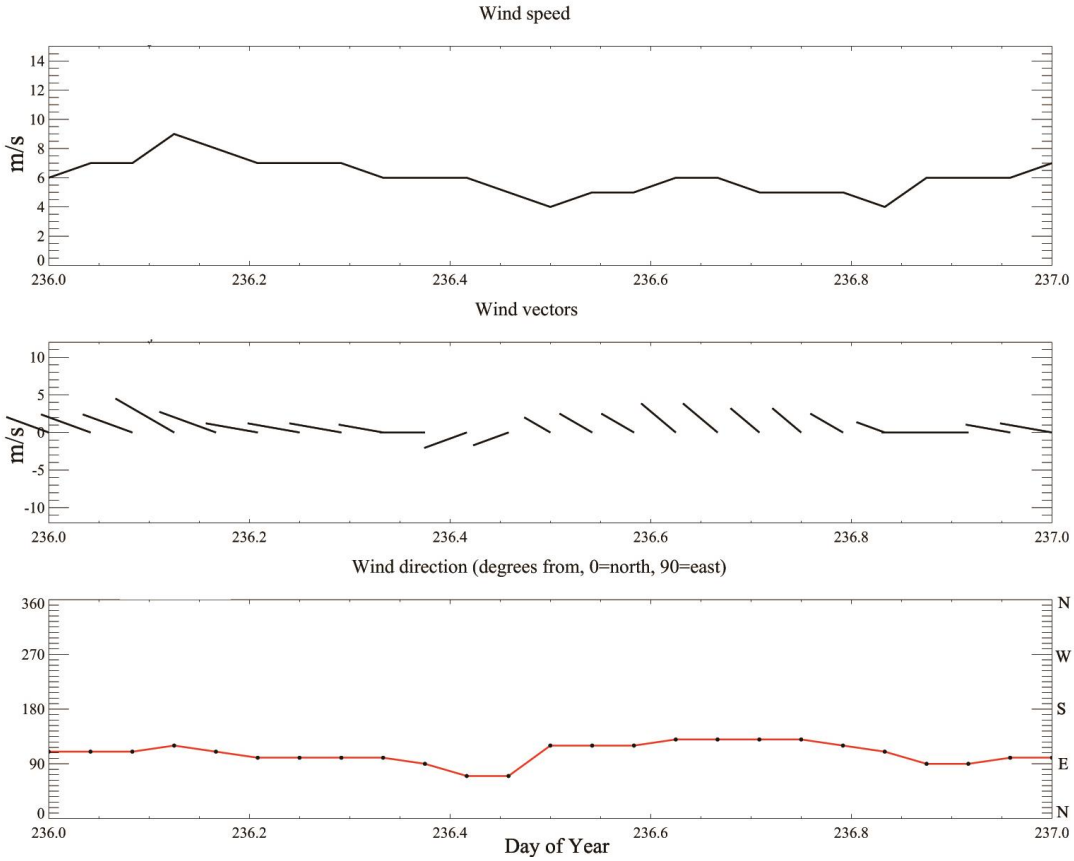

Observed hourly wind on August 24, 2014 (Day 236), buoy 45165

East wind (E)

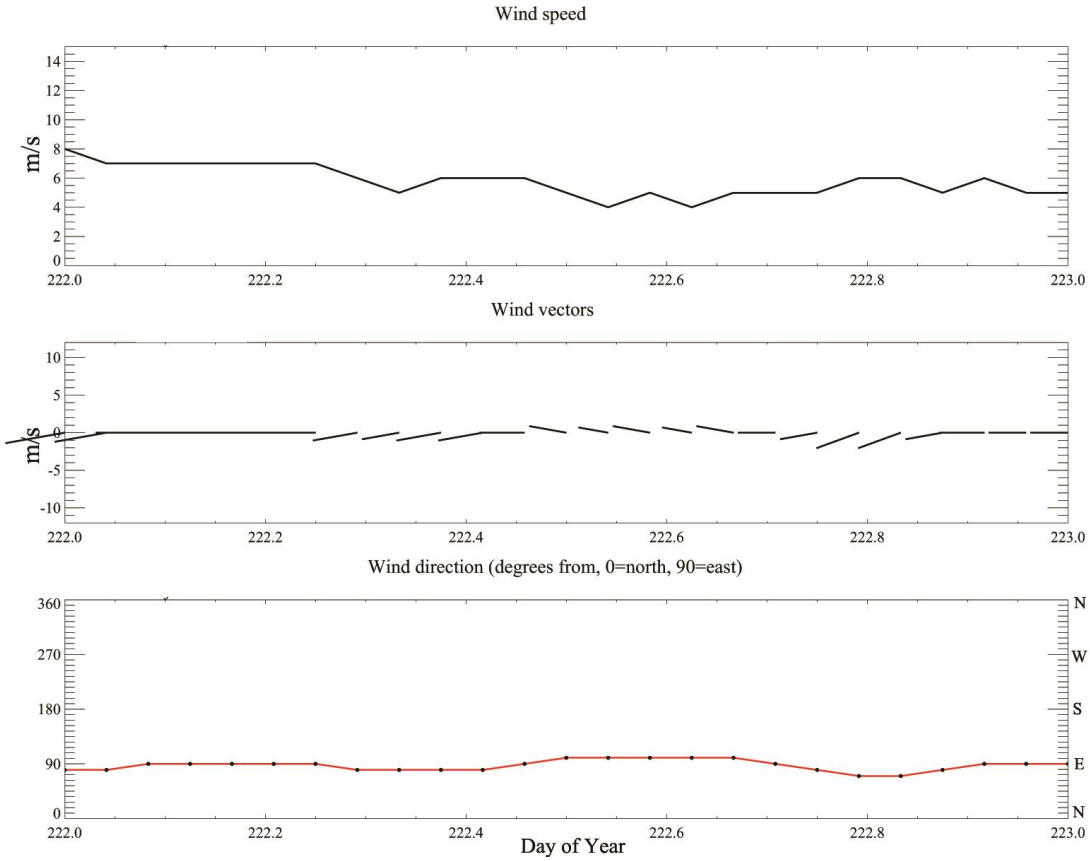

Observed hourly wind on August 10, 2014 (Day 222), buoy 45165

Northeast wind (NE)

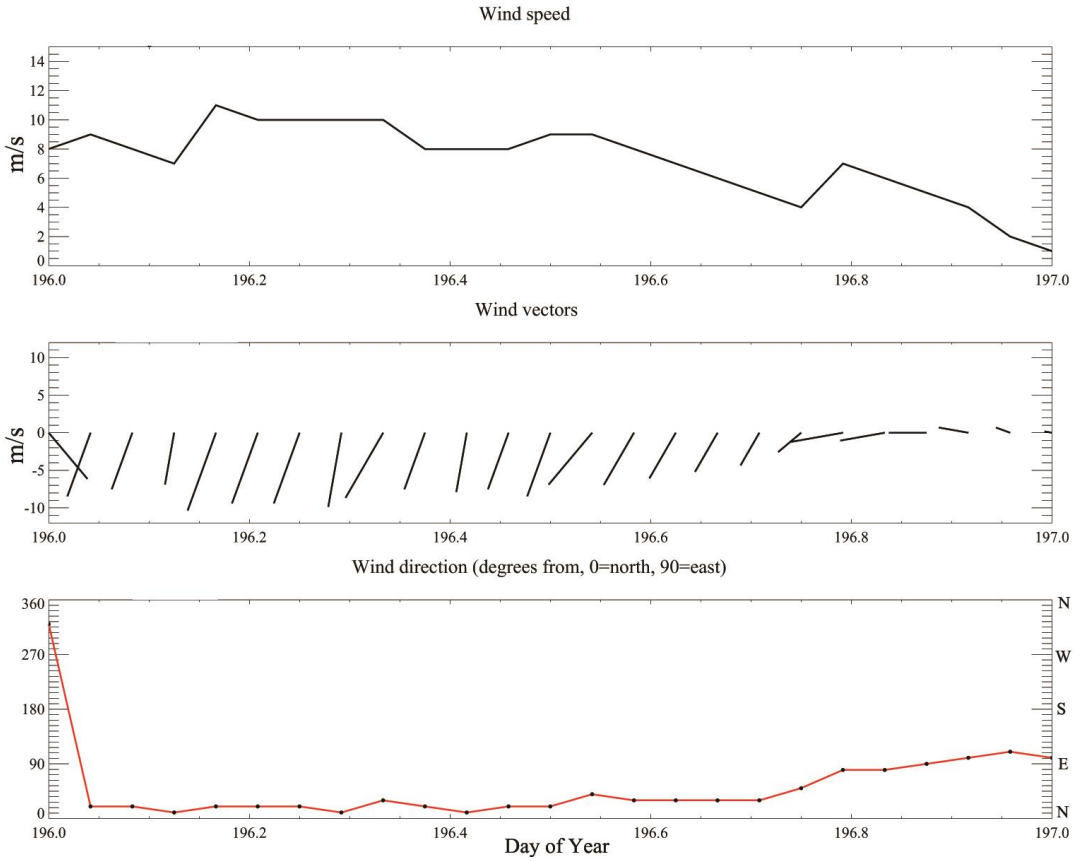

Observed hourly wind on July 30, 2015 (Day 196), buoy 45165

Appendix D. Circulation Patterns Produced by Winds of Various Directions (INTERP results)

North Wind (N)

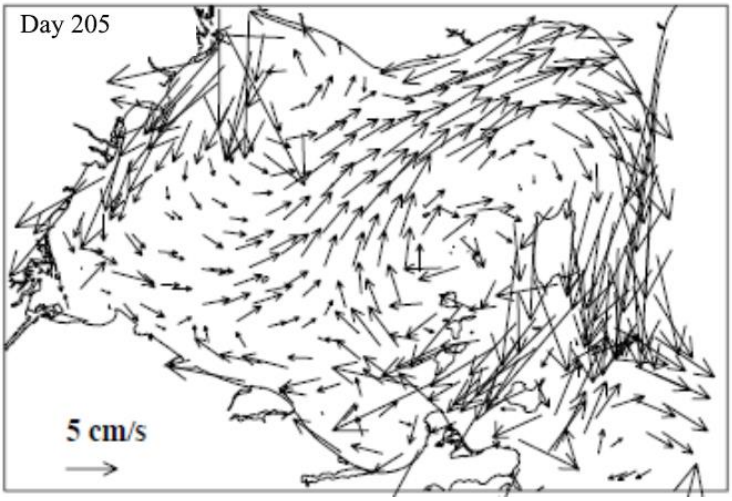

Depth-averaged circulation on July 24, 2014 (Day 205)

Northwest wind (NW)

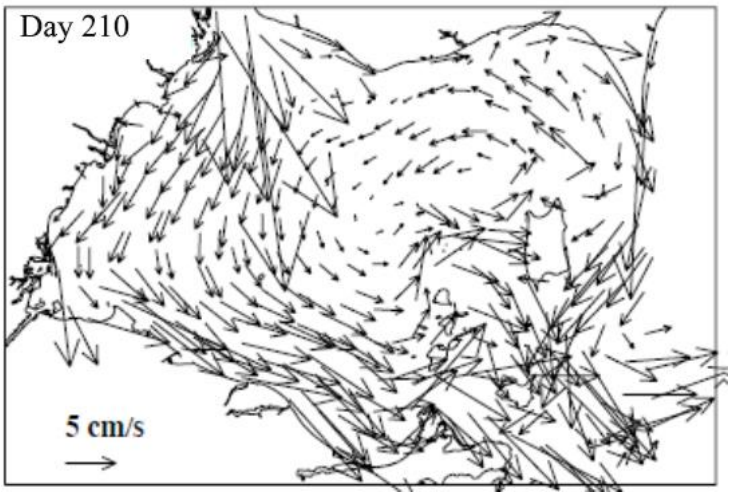

Depth-averaged circulation on July 29, 2014 (Day 210)

West wind (W)

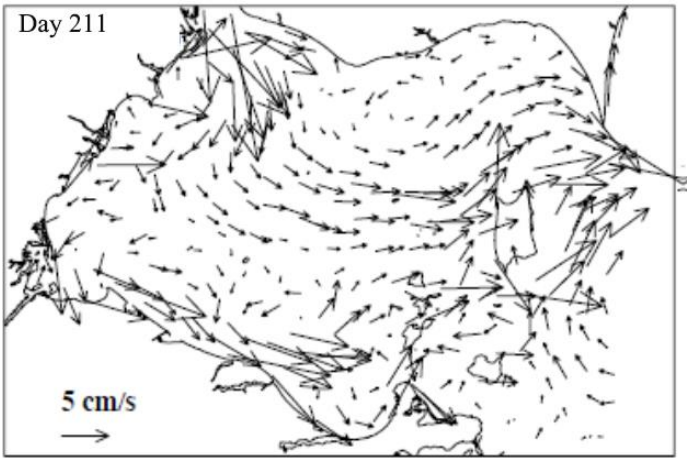

Depth-averaged circulation on July 30, 2015 (Day 211)

Southwest wind (SW)

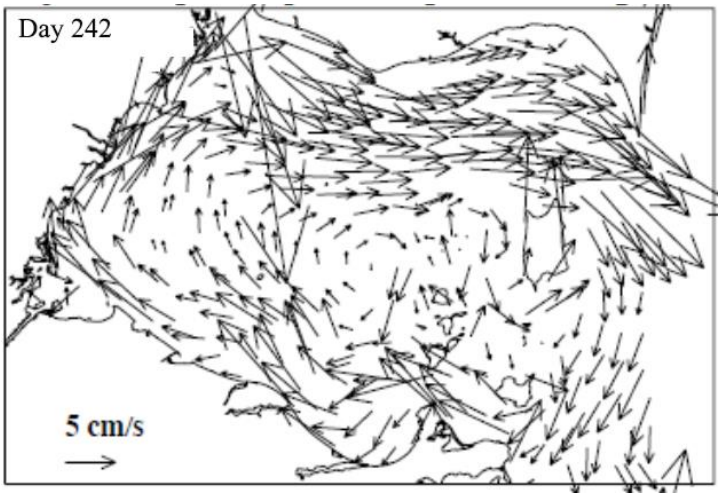

Depth-averaged circulation on August 30, 2014 (Day 242)

South wind (S)

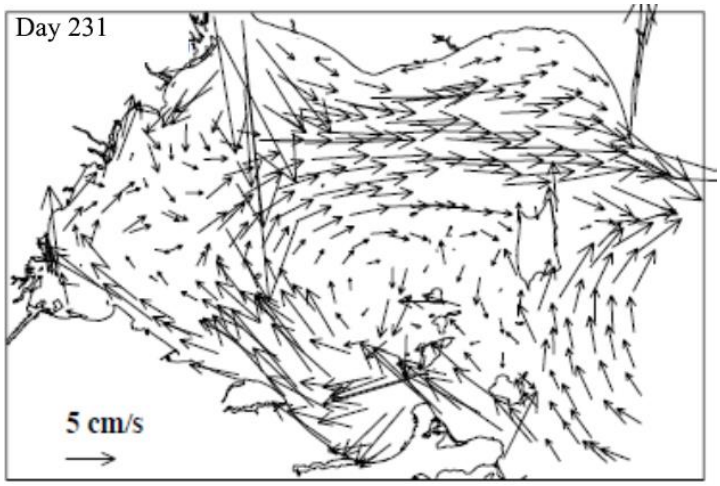

Depth-averaged circulation on August 19, 2015 (Day 231)

Southeast wind (SE)

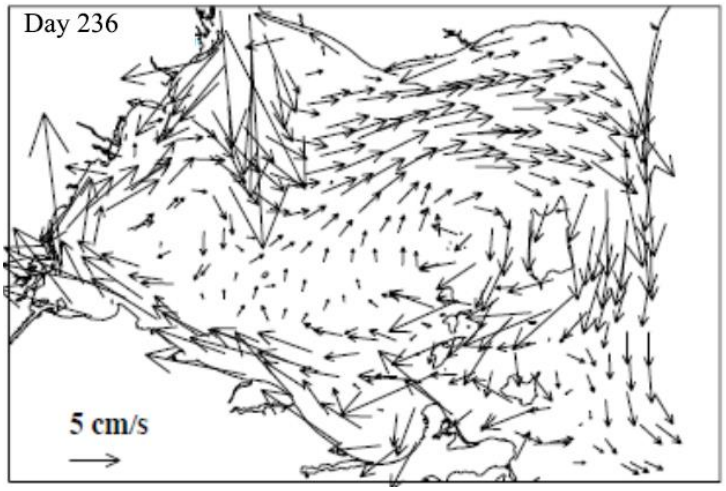

Depth-averaged circulation on August 24, 2014 (Day 236)

East wind (E)

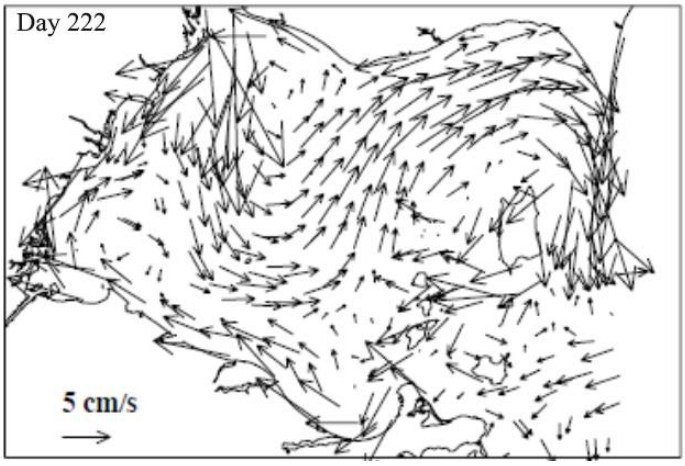

Depth-averaged circulation on August 10, 2014 (Day 222)

Northeast wind (NE)

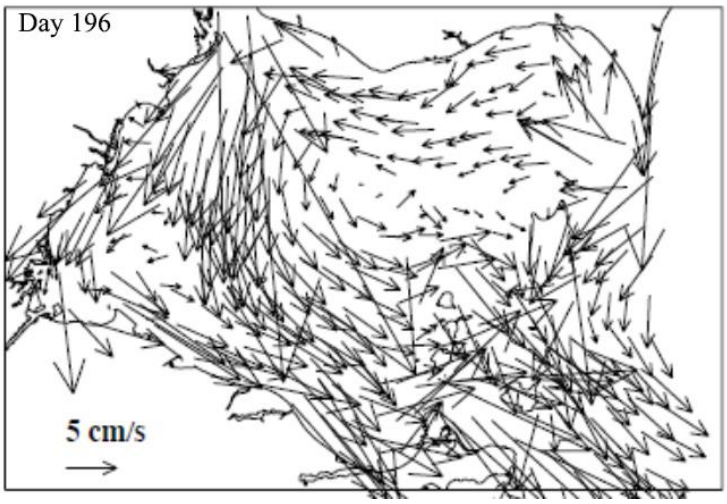

Depth-averaged circulation on July 15, 2015 (Day 196)